Concepts Toward a Global Mechanistic Mapping of Ocean Carbon Export

Emmanuel Laurenceau-Cornec, Mathieu Mongin, Thomas Trull, Matthieu Bressac, Emma Cavan, Lennart Bach, Frédéric Le Moigne, Frédéric Planchon, Philip Boyd

Global Biogeochemical Cycles

RESEARCH ARTICLE
10.1029/2023GB007742

Concepts Toward a Global Mechanistic Mapping of Ocean Carbon Export

Emmanuel C. Laurenceau-Cornec[1,2], Mathieu Mongin[3], Thomas W. Trull[4], Matthieu Bressac[5], Emma L. Cavan[6], Lennart T. Bach[1], Frédéric A. C. Le Moigne[2], Frédéric Planchon[2], and Philip W. Boyd[1]

[1]Institute for Marine and Antarctic Studies, University of Tasmania, Hobart, TAS, Australia, [2]Univ. Brest, CNRS, IRD, Ifremer, LEMAR, France, [3]CSIRO Oceans & Atmosphere, Coasts and Ocean Research Program, Hobart, TAS, Australia, [4]CSIRO Oceans & Atmosphere Climate Science Centre, Hobart, TAS, Australia, [5]Laboratoire d'Océanographie de Villefranche (LOV), Institut de la Mer de Villefranche, CNRS, Sorbonne Université, Villefranche-sur-Mer, France, [6]Department of Life Sciences, Imperial College London, Ascot, UK

Key Points:

- A plausible mechanistic map of ocean carbon export is derived from spatio-temporal changes in the e-ratio in mid- and high-latitude oceans
- The map unveils the possible distribution and boundaries of four main export systems and explains their potential ecological drivers
- The debated view that e-ratios vary mostly with latitude is challenged by results suggesting instead an effect of e-ratio seasonality

Supporting Information:

Supporting Information may be found in the online version of this article.

Correspondence to:

E. C. Laurenceau-Cornec,
emmanuel.laurenceaucornec@univ-brest.fr

Citation:

Laurenceau-Cornec, E. C., Mongin, M., Trull, T. W., Bressac, M., Cavan, E. L., Bach, L. T., et al. (2023). Concepts toward a global mechanistic mapping of ocean carbon export. *Global Biogeochemical Cycles*, *37*, e2023GB007742. https://doi.org/10.1029/2023GB007742

Received 21 FEB 2023
Accepted 23 AUG 2023

Author Contributions:

Conceptualization: Emmanuel C. Laurenceau-Cornec, Mathieu Mongin, Thomas W. Trull, Philip W. Boyd
Data curation: Emmanuel C. Laurenceau-Cornec, Mathieu Mongin, Matthieu Bressac, Emma L. Cavan, Lennart T. Bach, Frédéric Planchon
Formal analysis: Emmanuel C. Laurenceau-Cornec, Emma L. Cavan, Lennart T. Bach
Funding acquisition: Philip W. Boyd

Abstract The gravitational sinking of organic debris from ocean ecosystems is a dominant mechanism of the biological carbon pump (BCP) that regulates the global climate. The fraction of primary production exported downward, the e-ratio, is an important but poorly constrained BCP metric. In mid- and high-latitude oceans, seasonal and local variations of sinking particle fluxes strongly modulate the e-ratio. These locally specific e-ratio variations and their ecological foundations are here encapsulated in the term "export systems" (ES). ES have been partly characterized for a few ocean locations but remain largely ignored over most of the ocean surface. Here, in a fully conceptual approach and with the primary aim to understand rather than to estimate ocean carbon export, we combine biogeochemical (BGC) modeling with satellite observations to map ES at fine spatio-temporal scales. We identify four plausible ES with distinct e-ratio seasonalities across mid- and high-latitude oceans. The ES map confirms the outlines of traditional BGC provinces and unveils new boundaries indicating where (and how) the annual relationship between carbon export and production changes markedly. At six sites where ES features can be partially inferred from in situ data, we test our approach and propose key ecological processes driving carbon export. In the light of our findings, a re-examination of 1,841 field-based e-ratios could challenge the conventional wisdom that e-ratios change strongly with latitude, suggesting a possible seasonal artifact caused by the timing of observations. By deciphering carbon export mechanistically, our conceptual ES map provides timely directions to emergent ocean robotic explorations of the BCP.

Plain Language Summary The oceanic biological carbon pump regulates Earth's climate by carrying part of the dissolved CO_2 fixed by surface planktonic ecosystems to deeper depths. Controls that ecosystems exert on the fraction of carbon exported, the "e-ratio," have been partly identified at a few ocean locations, but are insufficient to achieve a global mechanistic understanding, especially where processes are affected by seasonality. Using a fully conceptual approach combining biogeochemical modeling and satellite observations, we map plausible e-ratio variations at an unprecedented resolution in the mid- and high-latitude oceans. The map unveils the possible distribution and boundaries of four main export systems and investigates their ecological drivers. Our work highlights long-standing inconsistencies from field-based e-ratios and provides a timely road map for emergent ocean robotic explorations.

1. Introduction

The ocean's biological carbon pump (BCP) consists of an ensemble of biologically-mediated processes that contribute to the uptake of atmospheric carbon and its storage in the deep ocean, thus mitigating global climate change (Boyd et al., 2019; Jin et al., 2020; Le Moigne, 2019; Volk & Hoffert, 1985). The suite of BCP processes starts in the sunlit surface ocean by the photosynthetic fixation of atmospheric CO_2 into organic matter. Then, part of the surface production is exported downward in the form of sinking organic particles representing the main—but not the only—pathway of the BCP (Le Moigne, 2019). In mid- and high-latitude oceans, surface net primary productivity (NPP) exhibits marked seasonal cycles that cause fluctuations in export flux. The exported fraction of NPP or "e-ratio"—commonly defined as the ratio of particulate organic carbon flux (C flux) at the base of the euphotic zone (Ez) to Ez-integrated NPP (Buesseler et al., 2020; Downs, 1989)—is a measure of

Investigation: Emmanuel C. Laurenceau-Cornec, Thomas W. Trull, Matthieu Bressac, Emma L. Cavan, Frédéric A. C. Le Moigne, Frédéric Planchon, Philip W. Boyd
Methodology: Emmanuel C. Laurenceau-Cornec, Mathieu Mongin, Philip W. Boyd
Project Administration: Emmanuel C. Laurenceau-Cornec
Resources: Emmanuel C. Laurenceau-Cornec, Mathieu Mongin, Thomas W. Trull, Frédéric A. C. Le Moigne, Philip W. Boyd
Software: Emmanuel C. Laurenceau-Cornec, Mathieu Mongin, Emma L. Cavan, Philip W. Boyd
Supervision: Emmanuel C. Laurenceau-Cornec, Mathieu Mongin, Thomas W. Trull, Philip W. Boyd
Validation: Emmanuel C. Laurenceau-Cornec, Mathieu Mongin, Thomas W. Trull, Matthieu Bressac, Lennart T. Bach, Frédéric A. C. Le Moigne, Frédéric Planchon, Philip W. Boyd
Visualization: Emmanuel C. Laurenceau-Cornec, Matthieu Bressac, Emma L. Cavan, Frédéric A. C. Le Moigne, Frédéric Planchon, Philip W. Boyd
Writing – original draft: Emmanuel C. Laurenceau-Cornec, Thomas W. Trull, Philip W. Boyd
Writing – review & editing: Emmanuel C. Laurenceau-Cornec, Mathieu Mongin, Thomas W. Trull, Matthieu Bressac, Emma L. Cavan, Lennart T. Bach, Frédéric A. C. Le Moigne, Frédéric Planchon, Philip W. Boyd

ocean carbon export efficiency. Despite the central importance of the e-ratio to assess how the BCP might be affected by ongoing changes of ocean ecosystems, its controls are still uncertain and the e-ratio remains difficult to predict because the magnitude and timing of C flux is influenced by many physical (Dall'Olmo et al., 2016; Omand et al., 2015) and ecological processes (Boyd & Newton, 1995; Cavan et al., 2017; Le Moigne et al., 2015) varying spatio-temporally.

Over the course of a year, the C flux generated by a surface planktonic ecosystem can take on various forms of sinking particles such as individual phytoplankton cells, phyto-aggregates or zooplankton fecal pellets. The different categories of sinking particles often lead to contrasted e-ratios and exhibit seasonal successions, forming locally a specific set of carbon export features hereafter called an "export system" (ES). ESs are reasonably well-characterized only at a few ocean locations (Henson et al., 2019). The complex seasonal dynamics pertaining to each ES remain uncertain due to the scarcity of observations. Locally, the e-ratio is conventionally inferred from ∼2 to 4 multi-day sampling of C flux and NPP measured over a few weeks, and hence with a largely inadequate coverage to reveal any seasonality. This sampling bias could potentially explain why scatter plots of the e-ratio compiling global data sets of field-based NPP versus C flux reveal no relationship (Buesseler, 1998; Laws & Maiti, 2019).

At a given location, an annual plot of the e-ratio at a high (daily) resolution—as obtained from a numerical model—resembles a loop termed "export loop" (Figure 1). The "export loop" plot and its potential to improve our mechanistic understanding of ocean export processes was first introduced in 1998 by Wassmann (1998). Below are exposed the basic principles of this representation. We refer the readers to P. Wassmann's seminal article for a comprehensive overview. On an annual export loop plot, each of the 365 data points corresponds to a daily value of NPP plotted against its synchronous C flux. Hence, each point graphically represents the daily e-ratio at a specific location, so the overall path followed by the export loop over one full year—determining its final shape—encompasses all annual variations of the e-ratio. On this representation, e-ratios that remain constant over time (i.e., C flux and NPP vary at the same rate) form straight lines radiating from the origin. During periods of stable e-ratios, the export loop follows these radial lines, while during periods of e-ratio variations (i.e., C flux changes faster or slower than NPP), the export loop progresses from one radial line to another (Figure 1c). Export loops can reveal large seasonal excursions of the daily e-ratio away from the annual mean e-ratio line (Figure 1) (Brix et al., 2006; Henson et al., 2015). This finding has several ramifications. First, it reinforces the idea that sporadic ship-based observations skew the seasonal patterns ("Obs.," Figure 1c). Second, it points to the existence of optimal periods and frequency of sampling for both NPP and C flux (Ceballos-Romero et al., 2016) that would better capture e-ratio seasonality than near the NPP or C flux maxima when observations are often conducted. Targeting the annual C flux maximum is an adequate strategy to estimate the bulk of the annual C flux, but can be misleading if the objective is a mechanistic understanding of the system.

The succession of curves and straight segments of an export loop illustrates the sequence of the dynamical interactions between daily NPP and C flux that can be connected to the different seasonal phases of an ecosystem functioning (e.g., spring bloom, export event, etc.; Figure 1b). For instance, the curvature of the export loop onset, the so-called "retention line" (Figure 1c), is a robust diagnostic of the degree of phytoplankton biomass retention in the surface layer (Wassmann, 1998). Importantly, the idealized shape shown on Figure 1c must be seen as the "backbone" of an ES, revealed after a numerical smoothing to remove most short-scale variability, and constituting a tool for comprehension rather than quantitative estimation. In the ocean, short-scale variability of NPP and C flux hides the general structures of export loops, so only an averaging of NPP and C flux over adequate time and space would reveal such shapes. Figure 1d attempts at reconstructing two successive export loops (2002–2004) in the northwest North Pacific. To achieve this, in situ C flux data at 100 m from three nearby time series stations (K1, K2, and KNOT) (Kawakami & Honda, 2007) were plotted against satellite-derived NPP computed at the same sites (2003–2004 climatology; see Section 3.1 for data source and algorithm used). The two successive export loops obtained display slightly different trajectories but are both narrow and remain close to their (bi-annual) mean e-ratio line, suggesting a limited e-ratio seasonality.

In the present study, designed as a thought experiment and following a purely conceptual approach, we aim at reconstructing plausible export loops on a global scale and at high spatio-temporal resolution to improve our *mechanistic* understanding of global carbon export. Global biogeochemical models that are routinely used in combination with satellite products to *quantitatively* estimate global C fluxes (Nowicki et al., 2022; Siegel et al., 2014) are subjected to high computational costs and must often limit their spatio-temporal resolution at

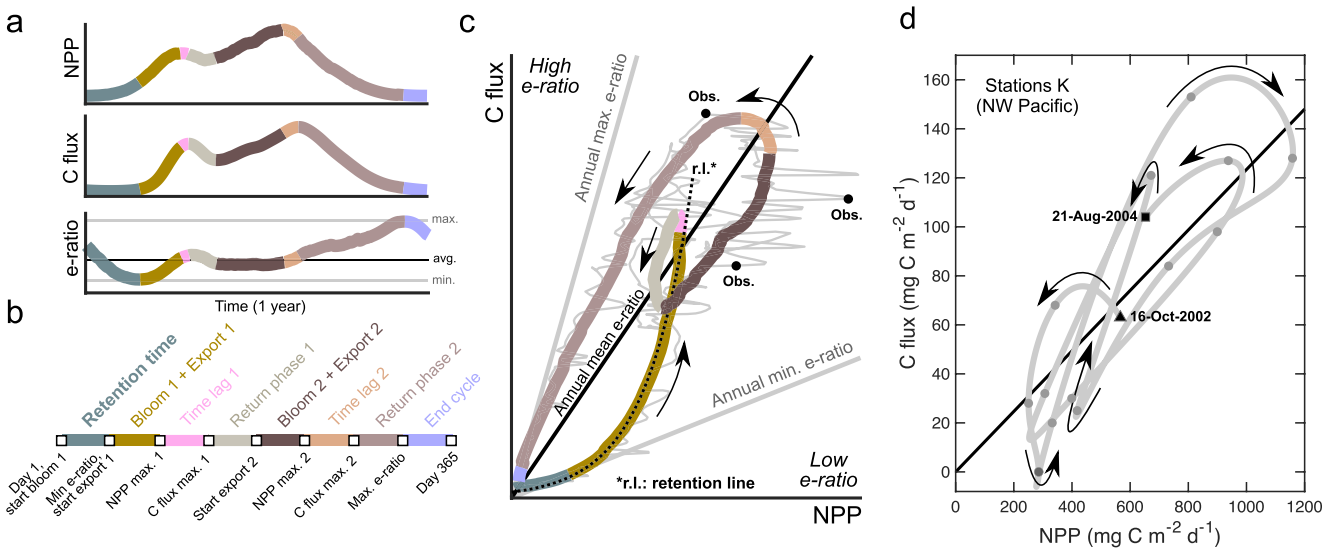

Figure 1. Anatomy of "export loops" from model simulations (a–c) and inferred from observations (d). An export loop (Wassmann, 1998) plots a time series of carbon flux (C flux) leaving the euphotic zone (Ez) against the Ez-integrated net primary productivity (NPP). Colors represent the sequential features in panels (a–c). (a) Seasonal fluctuations (spring to winter) of NPP, C flux and e-ratio (C flux:NPP) from a model simulation. (b) Nomenclature of sequential features including retention time (period of biomass accumulation within the Ez before C flux increases), the time lags between NPP and C flux maxima, and the return phase of the export loop when C flux decreases after export events. (c) Export loop plot from a model simulation. C flux plotted against NPP at high (daily) resolution forms an annual cycle not resolved by too sparse field observations ("Obs."). The structural shape is revealed after adequate smoothing (moving mean) of the raw data (thin gray line) affected by large short-scale variability. Constant e-ratios are straight lines radiating from the origin. The retention line (r.l.) is an exponential fit to the onset of the loop between the first day and NPP spring maximum ("NPP max. 1" on panel b) and provides a metric for biomass retention. Note the likelihood of large misestimation of the annual mean e-ratio depending on the timing of observations. (d) An observed export loop reconstructed from satellite-derived NPP and a time series of in situ C flux measured at 100 m at stations K (K1, K2, and KNOT) in the northwestern North Pacific between October 2002 and August 2004 (Kawakami & Honda, 2007).

the expense of their ability to reproduce locally complex seasonal signatures of planktonic ecosystem structure. Here, we follow a different approach which circumvents the potentially large uncertainties tied to a reconstruction of export loops at high spatio-temporal resolution that requires the simulation of realistic local ecosystem structure. Instead, in a conceptual (and thus less restricting) framework, we first simulate blindly numerous planktonic ecosystem structures with a generic biogeochemical model to randomly generate a statistical diversity of hypothetical export loops that could characterize most ESs across mid and high latitudes. Then, we assign each simulated export loop to its most plausible ocean location by comparing the NPP record for the simulated loop (NPP_{model}) to a local record of satellite-derived NPP (NPP_{sat}) used as a seasonal imprint of the subtle balance between biomass export and retention conditions. The central hypothesis motivating this thought experiment was that the seasonal variability of NPP_{sat} at a given site is sufficiently specific of the biomass retention versus export conditions to be used to identify the local ES. Because NPP_{sat} is partly inferred from phytoplankton biomass, its highly resolved (8-day) records over a year implicitly reflect the balance of productivity against loss terms including grazing and export (Arteaga et al., 2020). For this reason, a NPP_{sat} climatology at high resolution can encapsulate essential ecological features. The importance of NPP as a metric for ecosystem structure and carbon export flux parameterization has already been demonstrated (Dunne et al., 2005; Lutz et al., 2007; Schlenger et al., 2019), suggesting that it could be sufficiently specific to characterize ESs for different regions. In particular, the spatio-temporal variability of the relative dominance of small versus large phytoplankton groups, known to influence retention versus export conditions (Laurenceau-Cornec et al., 2015b; Mouw et al., 2016; Richardson, 2019), should be reflected in the main features of a NPP record (timing and amplitude of the maxima and minima, rates of increase and decrease).

Once all export loops were correctly assigned, the spatial distributions of four main ESs were inferred from a clustering analysis unveiling the transitions among distinctive retention line curvatures of these assigned export loops. Then, we tested the validity of our hypothesis using field observations at six selected sites and developed a mechanistic understanding of each ES. Finally, we use the results of this thought experiment to propose plausible links between planktonic ecosystem structures and e-ratio seasonality for each ES.

2. Materials and Methods

2.1. Physical Forcing of the CSIRO-EMS Biogeochemical Model

Simulations were performed using the generic CSIRO-EMS (Commonwealth Scientific and Industrial Research Organization, Australia-Ecological Modeling Suite) 3D coupled physical-biogeochemical model (Baird et al., 2020) forced with meteorological data from the Southern Ocean Time Series site (SOTS, 140°E, 47°S) (Trull et al., 2019) selected for its high-resolution observational framework and marked seasonality characteristic of most mid- and high-latitude waters. This model was chosen for its high flexibility and simple planktonic community structure applicable to a wide variety of environments. The physical module is the Sparse Hydrodynamic Ocean Code (SHOC) (Herzfeld, 2006). It is a finite difference hydrodynamic model resolving water velocity, temperature, salinity, density, passive tracers, mixing coefficients and sea level over three dimensions. SHOC is driven by inputs of winds, atmospheric pressure gradients, surface heat and water fluxes and has open boundary conditions. In the present study, SHOC was run for 9 years (2002–2011) at the SOTS site located between the Subtropical and Subantarctic fronts in the Southern Ocean (Orsi et al., 1995) and representative of a vast area of the Subantarctic zone (~90°E–140°E). The choice of the SOTS site was motivated by its extensive physical and biogeochemical data collection existing at high temporal resolution (hourly) provided by mooring facilities operated through the australian Integrated Marine Observing System (IMOS) (Eriksen et al., 2018; Trull et al., 2019; Wynn-Edwards et al., 2020), and thus directly available to our team for this experiment. Ranges of simulated seasonal variations of mixed layer depth (MLD: 9–785 m), and surface photosynthetic available radiation (PAR: 1.1–15 × 10^{-4} mol photons m^{-2} s^{-1}) approximate ranges of values averaged over the mid- and high-latitude oceans located between 30°N and 65°N and S (MLD (Schmidtko et al., 2013): 11–504 m; PAR: 1.6–5.1 × 10^{-4} mol photons m^{-2} s^{-1}). PAR and T for the mid- and high-latitude oceans were calculated from 2003 to 2020 NASA MODIS-Aqua climatologies (https://oceancolor.gsfc.nasa.gov/). The temperature range at SOTS (8.2–13.8°C in 2002–2011) did not cover the larger range of temperatures encountered in all mid- and high-latitude waters (0.7–26.4°C). A manual prescription of critical temperature-dependent rates (see details in Section 2.2) was made over extended ranges to ensure the applicability of our results over the whole mid- and high-latitude ocean.

2.2. Parameterization of the Biogeochemical Model

The biogeochemical module (Figure S1, Tables S1–S4 in Supporting Information S1) is a widely used generic model of plankton ecosystem dynamics (Baird et al., 2020). The present version is a Nutrient Phytoplankton Zooplankton Detritus model (two types for each compartment; Phytoplankton: P_a and P_b, Zooplankton: Z_a and Z_b) in which dissolved and particulate biogeochemical tracers are advected and diffused throughout the model grid in the same manner as temperature and salinity. Using a baseline set of parameters (Table S2 in Supporting Information S1) and initial conditions, the biogeochemical module was run for the first time over the whole SHOC simulated period (2002–2011). Then, 9 experiments—including 4 to 5 different simulations (totaling 38 simulations)—were run for the 2004–2008 time period using initial conditions from the base full-time simulation and 3 years between August 2004 and August 2007 were selected for their optimal steady state behavior and analyzed here. For each simulation, a single parameter constraining the ecosystem structure (bold in Table S2 in Supporting Information S1) and affecting directly or indirectly carbon export was varied incrementally: P_a and P_b linear mortality rates and sinking velocity, Z_a and Z_b swimming velocity (controlling grazing efficiency to the first order), the fraction of labile detritus converted to dissolved organic matter, the breakdown rate of labile detritus, and the parameterization of the sinking velocity for total detritus. Phytoplankton biomass retention was purposefully mediated via the dependence of detritus sinking velocity on the relative contributions of the two types of phyto- and zooplankton to detritus composition, and independently from particle size (Laurenceau-Cornec et al., 2015b) (Table S4 in Supporting Information S1). A constant sinking velocity of 320 m d^{-1} is attributed to zoo-detritus following Ploug et al. (2008) without distinction between small and large fecal material and dead bodies. The reconstructed particle flux was composed of mixed phyto-detritus and fecal matter, and thus had a large spectrum of sinking velocities (0–310 m d^{-1}) generating contrasting timescales of phytoplankton biomass retention within the Ez.

Key rates were varied over large ranges to ensure the applicability of our outputs to a large diversity of retention versus export conditions possibly encountered at mid and high latitudes. Our technique is applicable beyond the model regional boundaries owing to two fundamental features: (a) the ranges of the model physical components

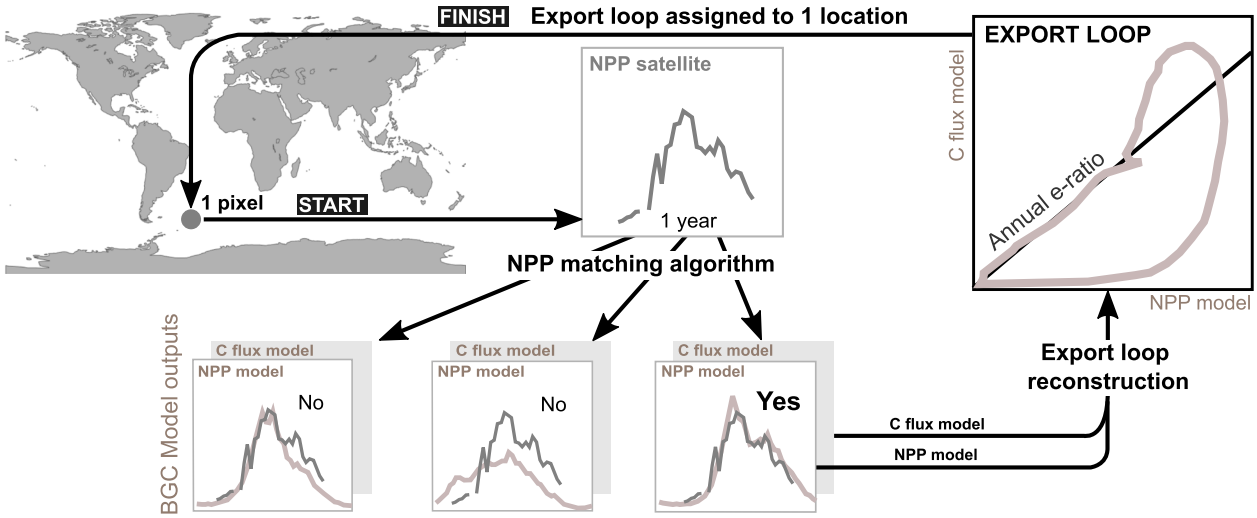

Figure 2. Diagram of the "net primary productivity (net primary productivity (NPP))—matching method" used to reconstruct maps of export loops and associated annual e-ratios, from the combination of satellite-derived NPP (NPP_{sat}) products and biogeochemical model outputs.

(MLDs and surface available radiations) are comparable to the ranges of values averaged over all mid- and high-latitude oceans where our analysis is conducted; (b) the use of a broad spectrum of physiological and ecological parameters permits to encompass most reported values for marine ecosystems (Baird et al., 2004; Bissinger et al., 2008; Eppley, 1972; Hansen et al., 1997; Hirst et al., 2003). Most ecological rates, including maximum growth rates, mortality rates, and remineralization rates are temperature-dependent in the BGC model (Baird et al., 2020). Manual prescription of these rates over larger ranges further ensured the applicability of our approach outside the limits of the regional model parameterization.

2.3. Reconstruction of Export Loops in Mid- and High-Latitude Oceans

For each of the 38 simulations, export loops were modeled at a daily resolution from Ez-integrated NPP and C flux at the base of the Ez sampled over a grid of 36 stations equally distributed across the regional model domain (Figure S2 in Supporting Information S1), so that a total of 4,104 export loops were generated (38 simulations × 36 stations × 3 years). Then, to determine which one among all generated export loops could best represent a specific ocean location, the annual record of NPP_{model} was matched to the most similar annual record of NPP_{sat} (2003–2018 satellite climatology resolved each 8-day; Section 3.1) in mid- and high-latitude waters (Figure 2).

The 46 "weeks" (8-day periods) of the satellite-derived NPP (NPP_{sat}) climatology (annual record with one value every 8 days) spatially-resolved at 1/4° were shifted backward or forward in time in order to re-center the local NPP_{sat} maxima on the exact middle of the year (week 23), thus synchronizing the annual cycle globally. Annual variations of NPP_{sat} were then matched with the most similar NPP_{model} variations. The optimal match was defined by the minimum sum of the absolute differences between satellite and simulated NPP calculated at each of the 46 weeks. Any consecutive 1-year record of NPP_{model} taken inside the 3 years of model runs was considered for the match, thus allowing any start time for the onset of the spring bloom. A given NPP_{model} record is thus the result of a specific set of model parameters but also depends on inter-annual variations of the initial (late winter) *P*/*Z* ratios.

The quality of the matching was evaluated through a series of filters. A coefficient of determination (r^2) greater than or equal to 0.6 and a *p*-value lower than or equal to 0.05 were arbitrarily fixed. Overall, the matching yielded a good correlation between NPP_{model} and NPP_{sat} at mid and high latitudes (Figure S3 in Supporting Information S1; mean coefficient of determination $r^2 = 0.73 \pm 0.16$ between 30°N and 65°N and S), and locally the NPP_{model} could mimic the NPP_{sat} with high accuracy. NPP_{sat} missing more than 15 weeks in the annual record due to cloud coverage were excluded. Regions south of 50°S and north of 60°N rarely feature more than 15 weeks of clear sky and therefore were not included in the analysis. We also excluded all NPP_{sat} records presenting less than 350 mg C m^{-2} d^{-1} in amplitude between annual minima and maxima, chosen as a minimum seasonality index. This seasonality index ensured the exclusion of regions where the annual NPP_{sat} presented little annual variation (i.e., where the match could have satisfied the r^2 limit despite a poor reproduction of NPP_{sat} seasonality).

10.1029/2023GB007742

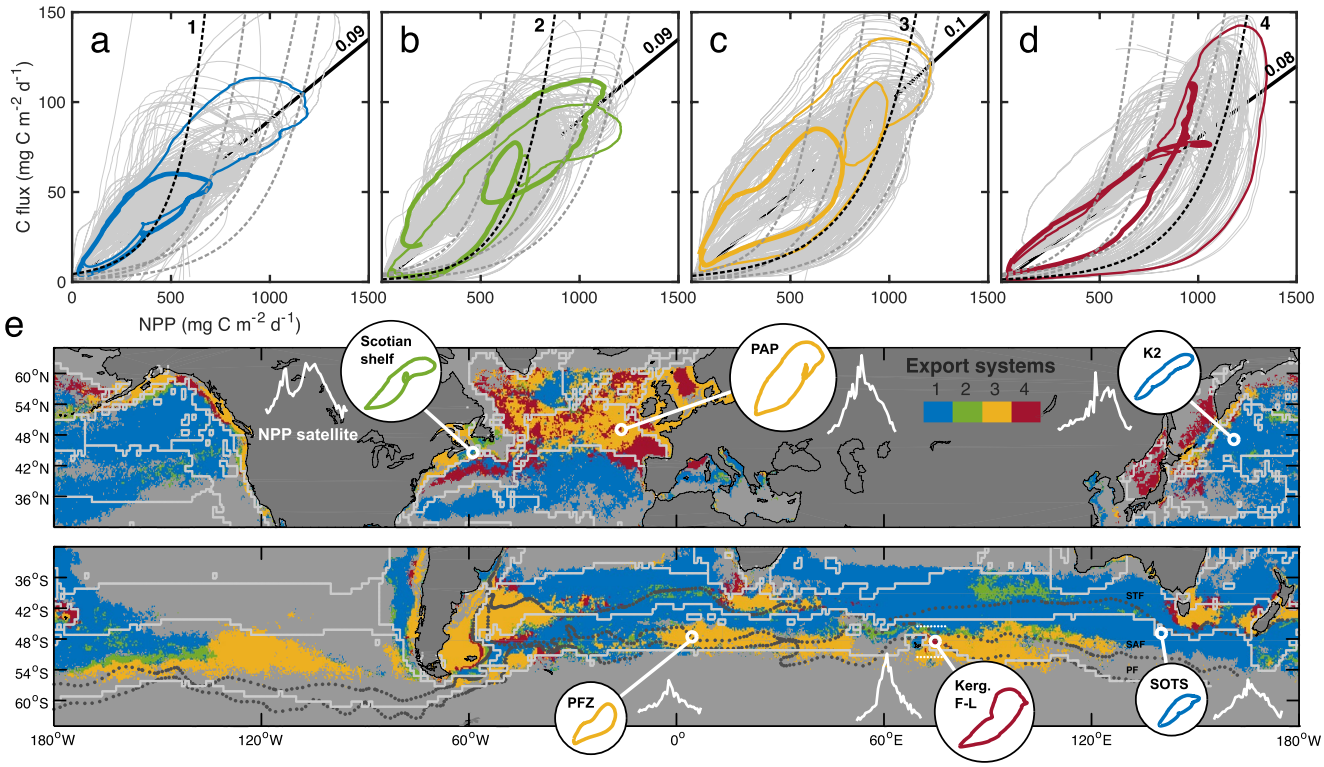

Figure 3. Identification and spatial distributions of the four main export systems (ESs) in the mid- and high-latitude oceans. (a–d) All reconstructed export loops grouped into four clusters (see Section 2.3) with distinctive morphologies (or "morphotypes") representative of four ESs; colored lines: topmost (thick), and second-most (thin) morphologies encountered in each cluster; gray lines: all other export loops sorted in each cluster; straight black line: mean annual e-ratio for each cluster (values indicated); dashed lines: mean best exponential fit to the onset of loop formation in each cluster referred to as the "retention line" (Figure 1). (e) Reconstructed spatial distribution of the four ESs for mid- and high-latitude ocean regions. Six case study sites are indicated: Scotian shelf, Porcupine Abyssal Plain (PAP), station K2, a Polar Frontal Zone (PFZ) site, the Kerguelen F-L station (KEOPS2 cruise), the Southern Ocean Time Series (SOTS) site. Light gray lines show the boundaries of dynamic biogeochemical provinces as defined by Reygondeau et al. (2013). Main Southern ocean fronts (Orsi et al., 1995) are also indicated; STF, SubTropical Front; SAF, SubAntarctic Front; PF, Polar Front. For each case study site, the annual cycle of NPP_{sat} and reconstructed export loop are shown as inserts (white lines; same scale for all sites). Grayed areas indicate a coefficient of determination of the NPP-matching method (Figure 2) lower than 0.6 or an incomplete record of the NPP_{sat}.

The NPP-matching method allowed us to reconstruct a plausible spatial distribution of all export loops at 1/4° resolution over the mid- and high-latitude waters (Figure S4a in Supporting Information S1). Over the vast choice of ~4,000 simulated export loops available to the matching routine, only a few morphologies were systematically returned as a best match, suggesting that a limited number of ESs operate at mid and high latitudes. Clustering of all spatialized export loops was made using the *kmedoids* function (Matlab, MathWorks Inc., version 2020a), which computes a *k-means* algorithm. It is likely that a continuum of retention line curvatures exists from systems with high retention to those with maximum export (Wassmann, 1998). The optimal number of clusters was fixed at 4 based on results from the *evalclusters* Matlab function (four evaluation criteria tested: *Calinski-Harabsz* criterion, *Davies-Bouldin* criterion, Gap value, Silhouette Value). Two metrics of the curvature of the retention line were used as inputs to the *kmedoids* function: the total NPP_{model} integrated between the start of the seasonal cycle and the start of the first export event (blue section on Figures 1a–1c), and the total NPP_{model} integrated between the start of the seasonal cycle and the day of maximum NPP of the spring bloom (blue section and khaki section on Figures 1a–1c). The clustering revealed four typical morphologies (Figures 3a–3d) or "morphotypes"—each corresponding to specific biomass retention versus export conditions (Figure S5 in Supporting Information S1). A conceptual map of the four ES (Figure 3e) was then obtained by attributing one color to the location (pixel) of each export loop sorted in one of the four clusters.

3. Data Sets

3.1. Satellite-Derived NPP Products

For this study, a suite of satellite-detection algorithms used for global estimates of marine primary production (Behrenfeld & Falkowski, 1997; Carr, 2002; Silsbe et al., 2016; Westberry et al., 2008) (CAFE, Carr, CBPM,

Eppley VGPM, Standard VGPM) was considered. Global NPP estimates (http://sites.science.oregonstate.edu/ocean.productivity) requiring full coverage result in part from a "cloud-filling" routine that artificially reconstructs NPP data based on neighboring values where clouds prevent satellite detection. The exclusive use of strict remotely-detected data was essential in this work. Ancillary data needed for NPP calculation (SST, surface chlorophyll *a*, PAR, and day length) were downloaded from the NASA Ocean color website (NASA Ocean Biology Processing Group, 2019; https://oceancolor.gsfc.nasa.gov/). The NPP was recalculated without cloud-filling between 2003 and 2018 for the Carr, VGPM, and Eppley algorithms. The Carr algorithm previously used in similar studies focusing on carbon export efficiency and noted for its good performance for carbon export reconstruction (Henson et al., 2011, 2019) gave the best results and was thus selected to build the 2003–2018 climatology (and 2003–2004 subset made specifically for Figure 1d) resolved each 8-day and used here.

3.2. In Situ C Fluxes and Inferred E-Ratios

A large global data set of 1,841 measurements of carbon fluxes made at 100 ± 75 m between 1988 and 2018 (Laurenceau-Cornec, 2023; Data Set S1) was built by combining several previously published data sets (Bisson et al., 2018; Henson, Sanders, & Madsen, 2012; Le Moigne, Henson, et al., 2013; Maiti et al., 2013; Mouw et al., 2016; Torres-Valdés et al., 2013), long time series (BATS, HOTS, CARIACO) and more recent studies. Carbon fluxes were derived from both the ^{234}Th tracer and traditional sediment trap methods. E-ratios corresponding to each C flux measurements were calculated as the ratio between measured C flux and NPP_{sat} estimated at the location of the flux measurements. This local NPP_{sat} was determined from the 8-day climatology averaged over a $0.5° \times 0.5°$ box centered on the exact location of the in situ C flux measurement. The period of the year corresponding to the C flux measurement was averaged over the collection time assumed at 16 days for ^{234}Th-derived fluxes (based on the ^{234}Th residence time (Henson et al., 2011)), and the deployment time for sediment trap-derived fluxes.

4. Results and Discussion

4.1. Plausible Carbon Export Systems in Mid- and High-Latitude Oceans

In our conceptual framework, the topmost and second-most frequently encountered export loops in each of the four clusters were considered representative of the plausible four main ES (ES1–4) that could dominate mid- and high-latitude oceans (Figure 3). Along with the retention line curvature we employed additional metrics of the level of phytoplankton biomass accumulation to interpret ecologically the differences among the ES morphotypes (Table 1): (a) The "retention time", that is, the number of days from the spring bloom onset (day 1) to the start of C flux increase; (b) the total NPP accumulated in the Ez from day 1 to the start of decline of the spring bloom; and (c) the rate at which the export loop progresses over the season gauged by the time elapsed from day 1 to the annual NPP maximum.

ES1 (Figure 3a) features a low retention of phytoplankton biomass and steady seasonal progression of the export loop (Table 1). ES2 (Figure 3b) appears as a transition to ES3 and ES4 (Figures 3c and 3d), which show higher retention of phytoplankton biomass as evidenced by the curvature of their retention lines, and rapid (then slow) seasonal progression of the export loop (Table 1; time to reach NPP max.). The degree of e-ratio seasonality is readily grasped visually from the area encompassed by the export loops, and was quantified here as the e-ratio annual range (difference max-min) and the root mean square error (RMSE) between daily and annual mean e-ratios. E-ratio seasonality differs greatly across the four ES (minimum e-ratio annual range of 0.15 for ES1 and maximum of 0.3 for ES3); yet annual mean e-ratios representing the overall export efficiencies appear very similar across all ES (Table 1).

4.2. Mechanistic Mapping of Ocean Carbon Export

Within each ES domain, the clustering gathered export loops that were generated with similar sets of model parameters, thus sharing comparable biomass retention versus export conditions (Figure S4b in Supporting Information S1). Most of the High Nutrient-Low Chlorophyll (HNLC) waters of the North Pacific and Southern Ocean are categorized as ES1, reflecting low phytoplankton biomass retention. ES3 and ES4—characterized by higher phytoplankton biomass retention—prevail in more productive regions (North Atlantic and coastal waters) and near Subantarctic fronts. ES2 occurs in coastal margins alongside ES3 and also offshore near Southern Ocean fronts. Interestingly, marked transitions between ES (ES1-ES3 or ES1-ES4) follow with particularly good agreement the overlaid boundaries of dynamic biogeochemical provinces accounting for seasonality in their definition

Global Biogeochemical Cycles

10.1029/2023GB007742

Table 1

Metrics of Export Systems and Seasonal Trends in Epipelagic Plankton Ecosystem Structure at Selected Sites: K2; SOTS: Southern Ocean Time Series; SCS: Scotian Shelf; PAP: Porcupine Abyssal Plain—Sustained Observatory; PFZ: Polar Frontal Zone; F-L: Station East of Kerguelen Island (KEOPS2)

	Export systems (ES)				Sites					
Metrics of export systems (reconstructed)	ES1	ES2	ES3	ES4	K2	SOTS	SCS	PAP	PFZ	F-L
(i) Retention time (days)	*20* (*3*)	15 (18)	**71 (14)**	50 (3)	*25*	*25*	34	58	**81**	61
(ii) Total accumul. prod. (g C m^{-2})	*15* (*0*)	24 (2)	32 (1)	**50 (5)**	*12.2*	15.7	25.7	35.1	31	**58.7**
(iii) Time to reach NPP max. (days)	**211 (11)**	192 (22)	190 (21)	*164* (*47*)	**239**	212	194	186	*175*	179
Annual mean e-ratio	0.1 (0)	0.1 (0.02)	**0.13 (0.02)**	*0.08* (*0.01*)	0.09	0.1	*0.08*	0.13	**0.14**	0.09
E-ratio annual range	*0.15* (*0.02*)	0.21 (0.08)	**0.3 (0.05)**	0.17 (0.02)	*0.15*	0.19	0.16	0.33	**0.34**	0.21
RMSE daily versus mean e-ratio	*13* (*3*)	17 (5)	**22 (4)**	16 (7)	*11*	*11*	13	**31**	19	18
% fecal matter in total detritus	**56 (3)**	21 (10)	*8* (*2*)	21 (3)	56	**59**	27	9	*7*	44

Seasonal trends in epipelagic plankton ecosystem structure (observed)[a]

Sites	Max. NPP_{sat} [*avg*]	Seasonal phytoplankton succession	Grazing pressure	C. flux composition
K2	1,256 [*510*]	Slow build up pico., diat., prym., dino.	Pico.	FA and rare PA
SOTS	840 [*415*]	Slow build up nano-, pico., prym., flag., diat.	Nano-, pico.	FA and rare PA
SCS	1,263 [*758*]	Early spring: diat. bloom; Summer: dino., nano-, pico.	Dino., nano., pico.	Non-packaged FM
PAP-SO	1,598 [*689*]	Early spring: diat. bloom; Summer: dino., cocco.	Dino., cocco.	PA, rare FP
PFZ	717 [*303*]	Spring: weak diat. bloom; All year: nano-, picofl.	Nano-, picofl.	Diat., FP-FA
F-L	1,376 [*526*]	Slow build-up large diat.; Spring-Summer: small diat. and dino.	Small diat., dino.	FP-FA, resting spores

Note. Metrics for the four export system morphotypes are presented as mean values (standard deviation in parentheses) extracted from the topmost and second-most frequently encountered export loop in each cluster (Figures 3a–3d). NPP: net primary productivity; NPP_{sat}: satellite-derived NPP (mg C m^{-2} d^{-1}); Total accumul. prod.: total net primary production accumulated in the euphotic zone during the first seasonal bloom from day 1 to the start of its decline; E-ratio annual range: difference between annual max. and min. e-ratio; RMSE: root mean square error relative to the annual mean e-ratio; nano-, pico.: nano- and picoplankton; nano-, picofl.: nano- and picoflagellate; diat.: diatoms; prym.: prymnesiophytes; dino.: dinoflagellates; flag.: autotrophic flagellates; cocco.: coccolithophorids; FA, FP, FM: fecal aggregates, pellets, matter; PA: phytodetrital aggregates. Highest and lowest values are indicated in bold and italics, respectively.

[a]Literature review is given in Supporting Information S1.

(Reygondeau et al., 2013). This result is consistent with our hypothesis that NPP records alone are sufficiently specific to distinguish between different ecosystem structures and could be used for their demarcation.

As stated above, the four ES domains (Figure 3e) were delimited by following the variations in retention line curvatures that are driven by both export features (reconstructed) and NPP seasonality (satellite-derived). Boundaries between each domain thus reflect the contrasting levels of phytoplankton biomass retention. This conceptual class of biogeochemical provinces is "process-based" and contrasts with bioregionalizations that use variables such as nutrient limitations (Moore et al., 2002), phytoplankton seasonality (Thomalla et al., 2011), or dominant phytoplankton groups (Alvain et al., 2008) rather than "whole-of-system" functions. Our model of ES based on NPP seasonality complements the traditional static biogeochemical provinces originally proposed by Longhurst (2007), and embeds in a single map a seasonally-dynamic definition of biogeochemical provinces (Reygondeau et al., 2013).

Across mid- and high-latitude waters, a comparison can be made between the degrees of biomass retention found within our plausible ES domains and other criteria traditionally used to delimit biogeochemical provinces. Differing levels of phytoplankton biomass retention can be observed within a single traditional biogeochemical province. For instance, the four ESs coexist inside the unique Sub-Antarctic Longhurst province (Longhurst, 2007; Reygondeau et al., 2013); conversely, distinct traditional biogeochemical provinces can share the same ES with similar conditions of biomass retention, such as in the North Pacific (Figure 3e). This suggests that a similarity of biogeochemical conditions (e.g., nutrient limitation) does not necessarily translate to a similarity of carbon export features. By shaping planktonic tropho-dynamics, seasonality introduces a higher degree of complexity in the selection of export pathways that is not easily captured by traditional biogeochemical provinces. In particular, zooplankton respond to seasonal successions of phytoplankton traits by adapted successions (Behrenfeld & Boss, 2014). The resulting variety of trophic interactions implies multiple export modes and efficiencies over the season.

4.3. Linking Ecosystem Structure and E-Ratio Seasonality

To date, no observational equivalent to our conceptual ES map is available, which precludes the application of our results to the real world. However, while the exactitude of the export loops reconstructed cannot be firmly verified, the agreement between the underlying processes that their shape implies and those observed in situ can be. The degree of biomass retention in the Ez can be evaluated quantitatively (in relative not absolute values) from our approach and (to the least) qualitatively through in situ observations of ecosystem structure and particle fluxes. In the ocean, particle retention in the Ez arises from low rates of particle loss relative to the increase in particle stocks. Particle loss can be hindered or delayed by the dominance of non- or slow-sinking phytoplankton, low rates of aggregation into larger and denser particles via physical coagulation (Jackson, 1990) or repackaging into fecal pellets by herbivory (Richardson & Jackson, 2007), intensive reprocessing/recycling by particle feeders and bacteria (Karl et al., 1988; Wexels Riser et al., 2007), or pronounced density gradients (Prairie et al., 2013) that stop settling particles. Six sites, each with optimal NPP matching (Figure 3e and Figure S6 in Supporting Information S1), were used to compare our conceptual results against real data on ecosystem structures providing insights into the degree of particle retention (Table 1, Text S2 and Figure S7 in Supporting Information S1).

At the low/moderate NPP_{sat} sites K2 (Honda et al., 2006) and SOTS (Trull et al., 2019) (ES1) our technique gives limited retention of phytoplankton biomass, slow seasonal progression of the export loop, and high fecal contributions to C flux (Table 1). Observations report a slow seasonal build-up of small phytoplankton species regularly grazed and resulting in a fecally dominated C flux (Boyd et al., 2008; Buesseler et al., 2008; Ebersbach et al., 2011; Eriksen et al., 2018; Fujiki et al., 2014; Halfter et al., 2020; Kobari et al., 2016; Matsumoto et al., 2014; Trull et al., 2008, 2019). At the Porcupine Abyssal Plain (PAP)—Sustained Observatory (PAP) (Hartman et al., 2012) and Polar Frontal Zone sites (Rutgers van der Loeff et al., 2011) (ES3) with high and low NPP_{sat}, respectively, our approach returns long phytoplankton biomass retention times, a NPP_{model} maximum rapidly reached, and phyto-detritus dominating the C flux. In situ data confirm the occurrence in early spring of short-lived blooms of heavily silicified diatoms, exported mostly as phyto-detritus, and smaller phytoplankton species dominating after spring and undergoing higher herbivory (Belcher et al., 2016; Cavan et al., 2019; Deppeler & Davidson, 2017; Ebersbach et al., 2011; Henson, Lampitt, & Johns, 2012; Joubert et al., 2011; Le Moigne, Boye, et al., 2013; Moore & Abbott, 2002; Roca-Martí et al., 2017; Siegel et al., 2002; Smythe-Wright et al., 2010). At the Scotian shelf (SCS) site (Charette et al., 2001) (ES2) field observations point to a system comparable to PAP but with a larger initial bloom: in early spring, a rapid and intense diatom bloom is followed by a limited summer bloom of small species under grazing control with rapid surface recycling (Cosper & Stepien, 1984; Craig et al., 2015; Ross et al., 2017; Ruckdeschel et al., 2020). All recon-

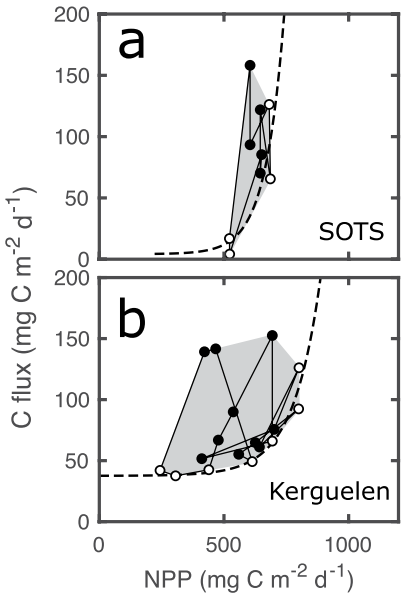

Figure 4. Plots of NPP_{sat} and in situ C fluxes measured at 100 ± 75 m available in 6 × 6° boxes centered on (a) the Southern Ocean Time Series (SOTS) station (47°S, 140°E), and (b) the Kerguelen F-L station (48.5°S, 74.7°E). One outlier (C flux >450 mg C m^{-2} d^{-1}) was excluded (panel b). Lines between datapoints indicate their connection in time. Only 23% (SOTS) and 44% (Kerg. F-L) of the complete annual cycles are covered, but note the differences in their assumed retention lines (dashed lines; exponential to white datapoints) and shape of the areas covered by the data sets (gray).

structed metrics at SCS agree with these features. At the Kerguelen F-L station (Laurenceau-Cornec et al., 2015a) (ES4) in situ data report a highly productive bloom over spring-summer sustained by successions of small fast-growing diatoms and dinoflagellates, combined with a slow build-up of larger diatom stocks; observations suggest also that phytoplankton undergoes significant grazing but most of the sinking fecal material is reprocessed by zooplankton (fragmentation and coprophagy) (Christaki et al., 2015; Halfter et al., 2020; Lasbleiz et al., 2016; Quéguiner, 2013; Trull et al., 2015). The resulting C flux measured in situ is moderate and mainly comprises grazing-resistant resting spores (Rembauville et al., 2015). Estimations using our method are all compatible with these observations: long retention times, conspicuous biomass accumulation in the Ez, and a fecally-dominated C flux (Table 1).

In addition, two partial reconstructions of field-based export loops were attempted for the SOTS and Kerguelen F-L stations (Figure 4)—that is, two sites suspected to present large contrasts in biomass retention—using NPP_{sat} and in situ C fluxes (100 ± 75 m; Section 3.2) available in 6° × 6° boxes centered on both sites. Although the time span of observations is largely insufficient to reconstruct whole annual cycles (only 23% and 44% covered at SOTS and Kerguelen F-L, respectively), significant differences between the two sites appear that tend to support our findings. In particular, the curvatures of the plausible retention lines, here defined *sensu lato* as structural baselines for the export loops (Wassmann, 1998), seem to confirm larger biomass retention at F-L than SOTS. Also, the contrasted scattering of the two C flux versus NPP data sets (gray areas on Figure 4; narrow for SOTS and wide for F-L) appears compatible with the differences in the shape of their respective reconstructed export loops (Figure 3e).

Overall, our hypothetical reconstructions agree with the observed differences between contrasted systems such as the HNLC (SOTS) site versus the Fe-Fertilized (F-L Kerguelen) station, or the North Atlantic bloom (PAP) site versus the oligotrophic North Pacific (K2). Our method suggests a much higher biomass retention (retention time and total accumulated production; Table 1) at PAP and F-L than at K2 and SOTS. Our results also support a plausible higher e-ratio seasonality at PAP and F-L than at SOTS and K2 (RMSE; Table 1). The observed contrasts in the grazing activity, limited at the North Atlantic PAP site and intense at the Kerguelen F-L station, are also reproduced accurately by our method (% fecal matter in total detritus; Table 1).

In general, real in situ observations and our conceptual results converge and suggest an important role played by zooplankton grazing in defining ES seasonal signatures. However, our BGC model, like several others addressing similar questions (Gorgues et al., 2019; Henson et al., 2015; Siegel et al., 2014), features simple tropho-dynamics and could lack the complexity needed to ascertain that zooplankton grazing is the main process controlling biomass retention timescale. In particular, the technique used here implied that optimal NPP matches could occur regardless of the bottom-up versus top-down factors controlling NPP seasonal variations in the model and at the location considered (e.g., MLD shoaling, nutrient exhaustion, relief of grazing pressure, etc.) with potential consequences on the interpretation of the drivers of carbon export. For example, phytoplankton mortality from distinct processes such as grazing or nutrient exhaustion might lead to similar NPP trends but different underlying carbon export features. However, the composition of exported detritus necessarily reflects the nature of their source processes. For instance, the absence of fecal matter would tend to suggest limited top-down controls on the temporal dynamics of productivity. In order to validate our approach the composition of the reconstructed and observed exported material was thus carefully assessed to test the similarity of drivers between NPP_{sat} and the NPP_{model} selected as best match.

Figure 5 summarizes the linkages between planktonic community structure, ESs and e-ratio seasonality by detailing the sequence from surface productivity, resulting C flux, and associated export loops. While this proposed scheme has solid foundations for (a) the shown contrasts in biomass retention and e-ratio seasonality, and (b) the planktonic seasonal succession and sinking particle fluxes, it can only remain speculative on their connections. We believe that the thorough literature review conducted here (Text S2 in Supporting Information S1) allowed us to characterize each system to the highest possible accuracy, and further evaluation would require more detailed and specifically-targeted observations.

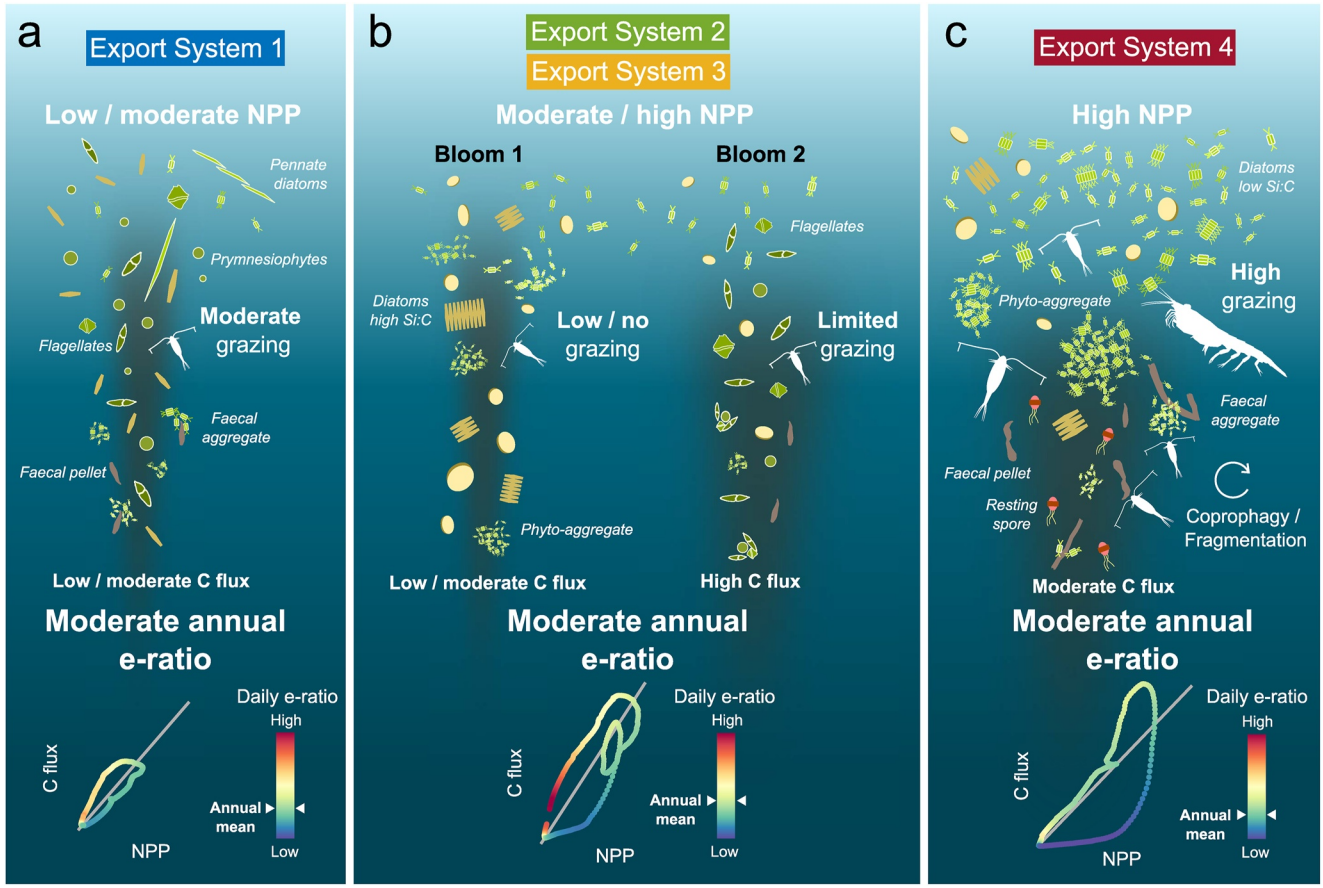

Figure 5. Proposed concepts of the relationships between epipelagic plankton community structure, export systems (ESs) and e-ratios. (a) ES1. In low- to moderately-productive waters (e.g., High Nutrient-Low Chlorophyll regions), prymnesiophytes and flagellates dominate along with larger pennate diatoms. Microzooplankton herbivory targets small species and is well adapted to low rates of net primary productivity increase. The carbon export flux (C flux) is low to moderate and mainly composed of fecal aggregates and a few large phytodetrital aggregates. This ES is stable, with little e-ratio variability and has a moderate annual mean e-ratio. (b) ES2, 3. In moderate- to highly-productive waters (e.g., North Atlantic and SO fronts), two distinct bloom events occur annually. The first bloom, generally dominated by heavily-silicified diatoms, is not (moderately) grazed ("silica body armor" and/or tropho-dynamic decoupling) and contributes little to the carbon export flux due to the high Si:C ratio. Biomass accumulation of the second bloom, dominated by flagellates, exceeds grazing and leads to a high carbon export flux. Seasonal variations of the e-ratio are high, but the annual mean e-ratio remains moderate. (c) ES4. In highly-productive waters, the spring-summer bloom is the main phytoplankton growth period and the autumnal bloom is a lesser event. The phytoplankton community is driven by successional trends of fast-growing diatoms undergoing high grazing pressure (lightly silicified). Many fecal pellets, fecal aggregates and phyto-detritus are produced, but their downward export is limited by high zooplankton reprocessing (e.g., fragmentation, coprophagy). Most of the remaining C flux consists of diatom resting spores. The annual mean e-ratio and its seasonal variability are both moderate.

Our conceptual approach yields significant differences in e-ratio seasonality across ESs, but annual mean e-ratios appear consistently invariant across sites (mean of all six sites: 0.11 ± 0.02). Limited variations of the annual mean e-ratio imply a balance over the year between processes that attenuate the C flux when NPP is high or enhance the C flux when NPP is low. In the real world, among the various mechanisms thought to influence biomass retention, zooplankton grazing is an essential driver. Zooplankton act as "gatekeepers" thought to modulate the efficiency of carbon export (Cavan et al., 2017; Halfter et al., 2020; Henson et al., 2022; Schmoker et al., 2013; Steinberg & Landry, 2017) in a complex fashion, at times facilitating the export flux and at times hindering it. Grazing on small cells could drive a significant carbon export via the production of small fecal pellets (Irion et al., 2021; Richardson & Jackson, 2007) in most mid- and high-latitude waters (ES1), contradicting the conventional view that small phytoplankton are rapidly recycled in the surface ocean. In contrast, grazing on large fast-sinking phyto-detritus (ES4) and their incidental fragmentation can lead to attenuation of the C flux (Dilling & Alldredge, 2000).

4.4. Comparison With Field-Based Measurements of the E-Ratio

To date, the interpretation of field-based e-ratios that have been suggested to carry large uncertainties (Buesseler et al., 2020; Henson et al., 2015; Laws & Maiti, 2019), has not permitted to fully understand the links between

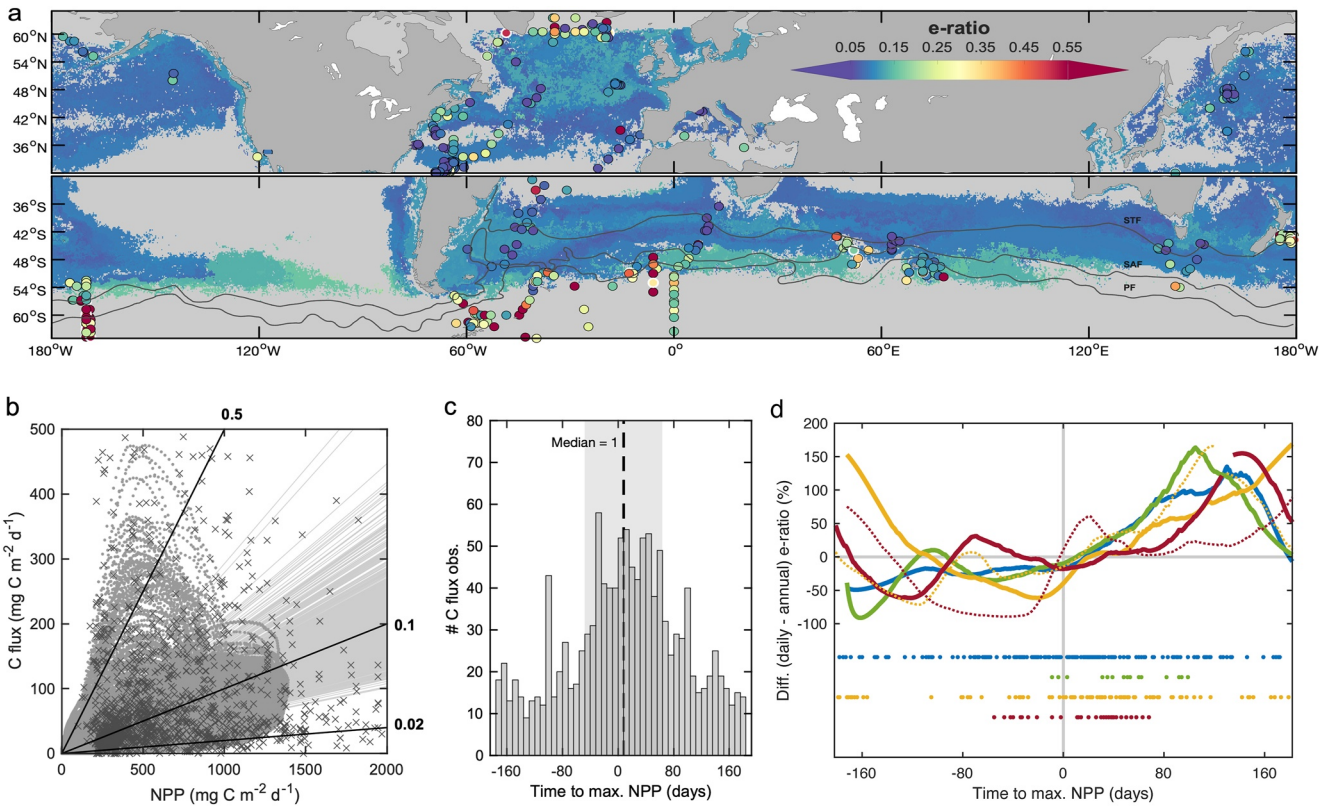

Figure 6. Comparison of hypothetical and observed e-ratios (a) Map of reconstructed annual mean e-ratios at 0.25° spatial resolution from simulated export loops in the mid- and high-latitude oceans. Dots represent field-based e-ratios—one observation or the average of several made at the same location (white circles: standard deviation of 0.1 or higher)—calculated from in situ C fluxes (100 ± 75 m) and satellite-derived net primary productivity (NPP_{sat}). Southern ocean fronts and grayed areas shown as per Figure 3. (b) Diversity of export loops (dots) and their annual mean e-ratio (gray lines) compared with field-based observations (crosses) of paired in situ C flux (100 ± 75 m) and NPP_{sat}. 7% of all observations lie outside the plot limits; black lines denote e-ratios of 0.02, 0.1, and 0.5. (c) Global in situ C flux measurements binned by the time lag in 8-day periods between the day of C flux measurement and the day of local NPP_{sat} maximum; long multi-decadal time series (BATS, HOT, CARIACO) including a disproportionately large number of observations in the mid- and low-latitude ocean are not included. Gray area indicates a 56-day window centered on the NPP_{sat} maximum that contains 48% of observations (d) Annual variations of the difference between reconstructed daily and annual mean e-ratio for the export loop morphotypes of Figures 3a–3d (same color code as per Figures 3a–3d; thick solid and thin dashed lines: topmost and second-most frequently encountered morphologies respectively). Each loop is recentered on its maximum NPP. Missing sections are periods connecting the start of a cycle and the end of the preceding cycle and were excluded due to uncertainties on e-ratio values. Colored dots indicate the seasonal timing of all C flux observations sorted by the identified type of export loop. Horizontal and vertical gray lines represent zero difference between daily and annual e-ratio and the day of maximum NPP, respectively.

ecosystem structures and e-ratios. To complement our primary objective of a mechanistic understanding of carbon export, we re-evaluate a data set of 1,841 field-based e-ratios collected between 1988 and 2018 (Section 3.2; Supporting Information S1) in the light of the proposed ES concepts. Observed e-ratios are expected to differ from our reconstructed e-ratios (Figure 6a) on two aspects: the known effect of measuring C flux at fixed depth versus at the base of the Ez (Buesseler et al., 2020), and the key role of seasonality emerging from the comparison of short-term field measurements to reconstructed annually-integrated e-ratios (derived from export loops) on which we focus. The importance of seasonality in the variability of global carbon export efficiency has been investigated in a recent study (de Melo Viríssimo et al., 2022), and our results suggest that most e-ratio variability could be seasonally- rather than regionally-driven. First, field-based e-ratios vary in a much larger range than our reconstructed annual mean e-ratios that most frequently fall between 0.075 and 0.1 and remain lower than 0.225 (Figure S8b in Supporting Information S1). Very similar values of annual mean e-ratios are obtained with the satellite-based mechanistic model of Siegel et al. (2014), but higher values are found by Henson et al. (2015) (global mean of 0.22) using a full model-based approach (i.e., without satellite data). Henson et al. mentioned that their model tends to overestimate the e-ratio in the southerly Southern Ocean and in the equatorial upwelling regions; these waters are not included in our global annual mean e-ratio (our analysis covers the latitudes between 30° and 65°) explaining possibly this difference besides the realistic versus conceptual approaches. Second, when reconstructed *daily* e-ratios are considered—thus accounting for the effect of seasonality—a range

similar to the observations is found (Figure S8a in Supporting Information S1 and Figure 6b). Finally, the median e-ratio is 0.1 regardless of data origin (daily vs. annual, reconstruction vs. observations; Figures S8a and S8b in Supporting Information S1).

Decades of observations reported greatest e-ratio values at high latitudes (Figure S8c in Supporting Information S1)—71% of observed e-ratios >0.4 are found at latitudes higher than 50°—supporting the idea that (part of) e-ratio variability is spatial. In the ocean, at high latitudes, high e-ratios are often related to blooms of large heavily-silicified diatoms (Friedrich & Loeff, 2002; Loeff et al., 1997) or other high and short export events (e.g., associated to retreating ice edge or polynyas, Amiel et al., 2002; Buesseler et al., 2003; Rutgers van der Loeff et al., 2011). Over mid- and high-latitude oceans, field-based e-ratios are temporally biased toward the timing of maximum NPP because measurements are often conducted in spring/summer. 48% of the C flux measurements considered here were conducted at the local NPP maximum ±56 days (Figure 6c).

We conceptually showed that along their seasonal trajectories, export loops can approach the annual mean e-ratio or largely depart from it (Figure 1), suggesting that high e-ratios frequently observed at high latitudes are short-term deviations from more moderate annual mean e-ratios. This hypothesis could not be verified here because of the incomplete NPP_{sat} record due to frequent cloudiness in these regions. However, our analysis suggests that the difference between daily and annual mean e-ratio varies over time as a function of the ES (Figure 6d), implying differing optimal sampling times of NPP and C flux to approach the annual mean e-ratio. Based on their location we classified all C flux measurements into their respective plausible ES and assessed if they could correspond to periods of high or low departure of daily e-ratios from their annual mean (Figure 6d). When considering the four topmost frequently-encountered export loop, results suggest that 48% of field-based e-ratios deviate from our hypothetical annual mean by at least 19%, and that 9% of these measurements provide a close (<5% difference) estimation of the reconstructed annual e-ratio.

Based on the conceptual ES morphotypes, high e-ratio variability occurs on average 20 days (SD = 5 days) before the spring NPP maximum, while e-ratios appear much steadier over the summer/fall regardless of the ES (Figure S9 in Supporting Information S1). For regions reaching their annual NPP maximum during the spring bloom (ES4), large differences between daily and annual mean e-ratio are thus expected near the NPP maximum (Figure 6d). On the contrary, ES for which the summer bloom is the main growth period present few variations of their e-ratio near their NPP maximum. E-ratio measurements made at any time of the year inside HNLC regions (ES1) are likely to be close to the annual mean, whereas measurements in bloom systems are subjected to much larger uncertainties. This is of particular importance given that most research attention is directed toward productive systems.

4.5. Uncertainties and Limits of the Approach

It must be stressed that the export loops reconstructed, the ES map inferred, and the concepts developed here are hypothetical and indicate the plausible contrasts of export versus retention conditions in the mid- and high-latitude oceans. Our conceptual approach did not aim at providing a predictive tool for carbon export, but at making a first step toward the identification of the general boundaries of ESs in the ocean. Uncertainties are inherent to the hypothesis tested, that is, an NPP annual record holds enough ecosystem and environmental characteristics to be used to unveil the spatial boundaries of the ESs. In particular, the diversity of biotic and abiotic processes that shape the productivity versus export relationships at different locations in the ocean can potentially lead to similar export loops but through different pathways. As a consequence, the features of each ES morphotype cannot be considered as exact representations of export loops that would be derived from in situ observations. While the qualitative comparison of our results with extensive observations collected at six ocean sites tend to validate our hypothesis, only future investigations of the seasonal relationship of NPP versus C flux at high resolution will be able to validate or contradict the concepts advanced in this work.

5. Conclusion and Perspectives

The present study is a step toward reaching a mechanistic understanding of how carbon export might operate over the global ocean. The map of the four ESs proposed shows where (and how) carbon export might function, and identify the probable underlying ecological drivers. However, in order to capture the full regional dynamics of particle export, combined observations of depth-integrated NPP and upper ocean C flux must be conducted

globally, at high temporal resolution, and over the whole annual cycle. Large efforts are being put into the development of in situ autonomous platforms that can provide such spatial and temporal coverage. Profiling floats of the BGC-Argo array (Bittig et al., 2019) resolve the Ez depth and are now able to measure in situ oxygen production and respiration and derive NPP (Johnson & Bif, 2021). Expanding numbers of floats with bulk bio-optical sensors (e.g., the US-NSF GO-BGC Array Project) will provide information on particulate carbon abundance (e.g., optical traps linking particle images to carbon content (Durkin et al., 2021; Estapa et al., 2017)), and others with particle imaging sensors such as the miniaturized sixth generation of the Underwater Vision Profiler (UVP6-LP, Hydroptics) will be able to count, size, and identify particles and plankton (e.g., grazers) from the surface to the deep ocean.

The emergence of technologies to sample ocean productivity and biogeochemical fluxes at high spatio-temporal resolution opens the possibility to measure complete export loops globally. The Global Argo program mission with its 10-day repeat cycle—and optimum of 5–7 days targeted for its BGC-Argo component (Bittig et al., 2019)—can capture export loops at a resolution just sufficient to overcome biases inherent to ship-based observations. This brings within observational reach the link between tropho-dynamics of the planktonic seasonal successions, their different export pathways, and e-ratio seasonality. Such a mechanistic understanding of global carbon export would allow crucial assessments of how planktonic shifts, that have started to alter the BCP (Beaugrand et al., 2002; Bopp et al., 2005; Brun et al., 2019), might ultimately affect the Earth system.

Data Availability Statement

The C flux data set used here is provided in supplementary information (Data Set S1) and published under the Creative Commons Attribution 4.0 International licence at https://doi.org/10.5281/zenodo.8207286. Requests for the codes used for the analyses should be addressed to E.C.L-C. All ancillary data needed for the NPP_{sat} calculation (SST, surface chlorophyll *a*, PAR, and day length) were downloaded from the NASA Ocean color website (https://oceancolor.gsfc.nasa.gov/).

Acknowledgments
We thank Mark Baird (Commonwealth Scientific and Industrial Research Organization, CSIRO) for his support with the CSIRO-EMS model parameterization. We would like to acknowledge Robert O'Malley (administrator of the Oregon state productivity website) for his insightful remarks on the use of satellite-derived NPP products, and Kevin Friedland (National Marine Fisheries Service, NOAA) for kindly sharing data. We thank Malwenn Lassudrie, Sébastien Moreau, and Marion Fourquez for fruitful discussions. We thank the two anonymous reviewers for their judicious comments and suggestions that helped improve the manuscript. This study received support through funding from the Australian Commonwealth Cooperative Research Centres Program to the Antarctic Climate and Ecosystems (ACE) CRC, and from the Australian National Network in Marine Science via the Institute for Marine and Antarctic Studies (IMAS, University of Tasmania). Tom Trull and the Southern Ocean Time Series received support from Australia's Integrated Marine Observing System (IMOS)—IMOS is enabled by the National Collaborative Research Infrastructure Strategy (NCRIS). This work was partly funded by the Australian Research Council through a Laureate awarded to Philip W. Boyd (FL160100131). Open access publishing facilitated by University of Tasmania, as part of the Wiley - University of Tasmania agreement via the Council of Australian University Librarians.

References

Alvain, S., Moulin, C., Dandonneau, Y., & Loisel, H. (2008). Seasonal distribution and succession of dominant phytoplankton groups in the global ocean: A satellite view. *Global Biogeochemical Cycles*, *22*(3), GB3001. https://doi.org/10.1029/2007GB003154

Amiel, D., Cochran, J. K., & Hirschberg, D. J. (2002). 234Th/238U disequilibrium as an indicator of the seasonal export flux of particulate organic carbon in the North Water. *Deep Sea Research Part II*, *49*(22), 5191–5209. https://doi.org/10.1016/S0967-0645(02)00185-6

Arteaga, L. A., Boss, E., Behrenfeld, M. J., Westberry, T. K., & Sarmiento, J. L. (2020). Seasonal modulation of phytoplankton biomass in the Southern Ocean. *Nature Communications*, *11*(1), 5364. https://doi.org/10.1038/s41467-020-19157-2

Baird, M. E., Oke, P. R., Suthers, I. M., & Middleton, J. H. (2004). A plankton population model with biomechanical descriptions of biological processes in an idealised 2D ocean basin. *Journal of Marine Systems*, *50*(3–4), 199–222. https://doi.org/10.1016/j.jmarsys.2004.02.002

Baird, M. E., Wild-Allen, K. A., Parslow, J., Mongin, M., Robson, B., Skerratt, J., et al. (2020). CSIRO environmental modelling suite (EMS): Scientific description of the optical and biogeochemical models (vB3p0). *Geoscientific Model Development*, *13*(9), 4503–4553. https://doi.org/10.5194/gmd-13-4503-2020

Beaugrand, G., Reid, P. C., Ibañez, F., Lindley, J. A., & Edwards, M. (2002). Reorganization of North Atlantic marine copepod biodiversity and climate. *Science*, *296*(5573), 1692–1694. https://doi.org/10.1126/science.1071329

Behrenfeld, M. J., & Boss, E. S. (2014). Resurrecting the ecological underpinnings of ocean plankton blooms. *Annual Review of Marine Science*, *6*(1), 167–194. https://doi.org/10.1146/annurev-marine-052913-021325

Behrenfeld, M. J., & Falkowski, P. G. (1997). Photosynthetic rates derived from satellite-based chlorophyll concentration. *Limnology & Oceanography*, *42*(1), 1–20. https://doi.org/10.4319/lo.1997.42.1.0001

Belcher, A., Iversen, M., Giering, S., Riou, V., Henson, S. A., Berline, L., et al. (2016). Depth-resolved particle-associated microbial respiration in the northeast Atlantic. *Biogeosciences*, *13*(17), 4927–4943. https://doi.org/10.5194/bg-13-4927-2016

Bissinger, J. E., Montagnes, D. J. S., Harples, J., & Atkinson, D. (2008). Predicting marine phytoplankton maximum growth rates from temperature: Improving on the Eppley curve using quantile regression. *Limnology & Oceanography*, *53*(2), 487–493. https://doi.org/10.4319/lo.2008.53.2.0487

Bisson, K. M., Siegel, D. A., DeVries, T., Cael, B. B., & Buesseler, K. O. (2018). How data set characteristics influence ocean carbon export models. *Global Biogeochemical Cycles*, *32*(9), 1312–1328. https://doi.org/10.1029/2018GB005934

Bittig, H. C., Maurer, T. L., Plant, J. N., Schmechtig, C., Wong, A. P. S., Claustre, H., et al. (2019). A BGC-Argo guide: Planning, deployment, data handling and usage. *Frontiers in Marine Science*, *6*, 502. https://doi.org/10.3389/fmars.2019.00502

Bopp, L., Aumont, O., Cadule, P., Alvain, S., & Gehlen, M. (2005). Response of diatoms distribution to global warming and potential implications: A global model study. *Geophysical Research Letters*, *32*(19). https://doi.org/10.1029/2005GL023653

Boyd, P. W., Claustre, H., Levy, M., Siegel, D. A., & Weber, T. (2019). Multi-faceted particle pumps drive carbon sequestration in the ocean. *Nature*, *568*(7752), 327–335. https://doi.org/10.1038/s41586-019-1098-2

Boyd, P. W., Gall, M. P., Silver, M. W., Coale, S. L., Bidigare, R. R., & Bishop, J. L. K. B. (2008). Quantifying the surface-subsurface biogeochemical coupling during the VERTIGO ALOHA and K2 studies. *Deep Sea Research Part II: Topical Studies in Oceanography*, *55*(14–15), 1578–1593. https://doi.org/10.1016/j.dsr2.2008.04.010

Boyd, P. W., & Newton, P. (1995). Evidence of the potential influence of planktonic community structure on the interannual variability of particulate organic carbon flux. *Deep Sea Research Part I*, *42*(5), 619–639. https://doi.org/10.1016/0967-0637(95)00017-Z

Brix, H., Gruber, N., Karl, D. M., & Bates, N. R. (2006). On the relationships between primary, net community, and export production in subtropical gyres. *Deep Sea Research Part II: Topical Studies in Oceanography*, *53*(5–7), 698–717. https://doi.org/10.1016/j.dsr2.2006.01.024

Brun, P., Stamieszkin, K., Visser, A. W., Licandro, P., Payne, M. R., & Kiørboe, T. (2019). Climate change has altered zooplankton-fuelled carbon export in the North Atlantic. *Nature Ecology & Evolution*, *3*(3), 416–423. https://doi.org/10.1038/s41559-018-0780-3

Buesseler, K. O. (1998). The decoupling of production and particulate export in the surface ocean. *Global Biogeochemical Cycles*, *12*(2), 297–310. https://doi.org/10.1029/97GB03366

Buesseler, K. O., Barber, R. T., Dickson, M.-L., Hiscock, M. R., Moore, J. K., & Sambrotto, R. (2003). The effect of marginal ice-edge dynamics on production and export in the Southern Ocean along 170°W. *Deep Sea Research Part II*, *50*(3–4), 579–603. https://doi.org/10.1016/s0967-0645(02)00585-4

Buesseler, K. O., Boyd, P. W., Black, E. E., & Siegel, D. A. (2020). Metrics that matter for assessing the ocean biological carbon pump. *Proceedings of the National Academy of Sciences*, *117*(18), 9679–9687. https://doi.org/10.1073/pnas.1918114117

Buesseler, K. O., Trull, T. W., Steinberg, D. K., Silver, M. W., Siegel, D. A., Saitoh, S. I., et al. (2008). VERTIGO (VERtical transport in the global ocean): A study of particle sources and flux attenuation in the North Pacific. *Deep Sea Research Part II: Topical Studies in Oceanography*, *55*(14–15), 1522–1539. https://doi.org/10.1016/j.dsr2.2008.04.024

Carr, M.-E. (2002). Estimation of potential productivity in Eastern Boundary Currents using remote sensing. *Deep Sea Research Part II: Topical Studies in Oceanography*, *49*(1), 59–80. https://doi.org/10.1016/S0967-0645(01)00094-7

Cavan, E. L., Henson, S. A., Belcher, A., & Sanders, R. (2017). Role of zooplankton in determining the efficiency of the biological carbon pump. *Biogeosciences*, *14*(1), 177–186. https://doi.org/10.5194/bg-14-177-2017

Cavan, E. L., Laurenceau-Cornec, E. C., Bressac, M., & Boyd, P. W. (2019). Exploring the ecology of the mesopelagic biological pump. *Progress in Oceanography*, *176*, 102125. https://doi.org/10.1016/j.pocean.2019.102125

Ceballos-Romero, E., Moigne, F. A. C. L., Henson, S., Marsay, C. M., Sanders, R. J., García-Tenorio, R., & Villa-Alfageme, M. (2016). Influence of bloom dynamics on particle export efficiency in the North Atlantic: A comparative study of radioanalytical techniques and sediment traps. *Marine Chemistry*, *186*, 198–210. https://doi.org/10.1016/j.marchem.2016.10.001

Charette, M. A., Moran, S. B., Pike, S. M., & Smith, J. N. (2001). Investigating the carbon cycle in the Gulf of Maine using the natural tracer thorium 234. *Journal of Geophysical Research*, *106*(C6), 11553–11579. https://doi.org/10.1029/1999JC000277

Christaki, U., Georges, C., Genitsaris, S., & Monchy, S. (2015). Microzooplankton community associated with phytoplankton blooms in the naturally iron-fertilized Kerguelen area (Southern Ocean). *FEMS Microbiology Ecology*, *91*(7), fiv068. https://doi.org/10.1093/femsec/fiv068

Cosper, E., & Stepien, J. C. (1984). Phytoplankton-zooplankton coupling in the outer continental shelf and slope waters of the Mid-Atlantic Bight, June 1979. *Estuarine, Coastal and Shelf Science*, *18*(2), 145–155. https://doi.org/10.1016/0272-7714(84)90102-1

Craig, S. E., Thomas, H., Jones, C. T., Li, W. K. W., Greenan, B. J. W., Shadwick, E. H., & Burt, W. J. (2015). The effect of seasonality in phytoplankton community composition on CO_2 uptake on the Scotian Shelf. *Journal of Marine Systems*, *147*, 52–60. https://doi.org/10.1016/j.jmarsys.2014.07.006

Dall'Olmo, G., Dingle, J., Polimene, L., Brewin, R. J. W., & Claustre, H. (2016). Substantial energy input to the mesopelagic ecosystem from the seasonal mixed-layer pump. *Nature Geoscience*, *9*(11), 820–823. https://doi.org/10.1038/ngeo2818

de Melo Viríssimo, F., Martin, A. P., & Henson, S. A. (2022). Influence of seasonal variability in flux attenuation on global organic carbon fluxes and nutrient distributions. *Global Biogeochemical Cycles*, *36*(2), e2021GB007101. https://doi.org/10.1029/2021GB007101

Deppeler, S. L., & Davidson, A. T. (2017). Southern Ocean phytoplankton in a changing climate. *Frontiers in Marine Science*, *4*, 40. https://doi.org/10.3389/fmars.2017.00040

Dilling, L., & Alldredge, A. L. (2000). Fragmentation of marine snow by swimming macrozooplankton: A new process impacting carbon cycling in the sea. *Deep Sea Research Part I*, *47*(7), 1227–1245. https://doi.org/10.1016/S0967-0637(99)00105-3

Downs, J. (1989). *Export of production in oceanic systems: Information from phaeopigment carbon and nitrogen analyses* (PhD thesis). University of Washington.

Dunne, J. P., Armstrong, R. A., Gnanadesikan, A., & Sarmiento, J. L. (2005). Empirical and mechanistic models for the particle export ratio. *Global Biogeochemical Cycles*, *19*(4), GB4026. https://doi.org/10.1029/2004GB002390

Durkin, C. A., Buesseler, K. O., Cetinić, I., Estapa, M. L., Kelly, R. P., & Omand, M. (2021). A visual tour of carbon export by sinking particles. *Global Biogeochemical Cycles*, *35*(10), e2021GB006985. https://doi.org/10.1029/2021GB006985

Ebersbach, F., Trull, T. W., Davies, D. M., & Bray, S. G. (2011). Controls on mesopelagic particle fluxes in the sub-Antarctic and polar frontal zones in the Southern Ocean south of Australia in summer—Perspectives from free-drifting sediment traps. *Deep Sea Research Part II: Topical Studies in Oceanography*, *58*(21–22), 2260–2276. https://doi.org/10.1016/j.dsr2.2011.05.025

Eppley, R. W. (1972). Temperature and phytoplankton growth in the sea. *Fishery Bulletin NOAA*, *70*(4), 1063–1085.

Eriksen, R., Trull, T., Davies, D., Jansen, P., Davidson, A., Westwood, K., & van den Enden, R. (2018). Seasonal succession of phytoplankton community structure from autonomous sampling at the Australian Southern Ocean Time Series (SOTS) observatory. *Marine Ecology Progress Series*, *589*, 13–31. https://doi.org/10.3354/meps12420

Estapa, M., Durkin, C., Buesseler, K., Johnson, R., & Feen, M. (2017). Carbon flux from bio-optical profiling floats: Calibrating transmissometers for use as optical sediment traps. *Deep Sea Research Part I*, *120*, 100–111. https://doi.org/10.1016/j.dsr.2016.12.003

Friedrich, J., & Loeff, M. M. R. V. D. (2002). A two-tracer (^{210}Po–^{234}Th) approach to distinguish organic carbon and biogenic silica export flux in the Antarctic Circumpolar Current. *Deep Sea Research Part I*, *49*(1), 101–120. https://doi.org/10.1016/S0967-0637(01)00045-0

Fujiki, T., Matsumoto, K., Mino, Y., Sasaoka, K., Wakita, M., Kawakami, H., et al. (2014). Seasonal cycle of phytoplankton community structure and photophysiological state in the western subarctic gyre of the North Pacific. *Limnology & Oceanography*, *59*(3), 887–900. https://doi.org/10.4319/lo.2014.59.3.0887

Gorgues, T., Aumont, O., & Memery, L. (2019). Simulated changes in the particulate carbon export efficiency due to diel vertical migration of zooplankton in the North Atlantic. *Geophysical Research Letters*, *46*(10), 5387–5395. https://doi.org/10.1029/2018GL081748

Halfter, S., Cavan, E. L., Swadling, K. M., Eriksen, R. S., & Boyd, P. W. (2020). The role of zooplankton in establishing carbon export regimes in the Southern Ocean—A comparison of two representative case studies in the subantarctic region. *Frontiers in Marine Science*, *7*, 837. https://doi.org/10.3389/fmars.2020.567917

Hansen, P. J., Bjørnsen, P. K., & Hansen, B. W. (1997). Zooplankton grazing and growth: Scaling within the 2-2,000 µm body size range. *Limnology & Oceanography*, *42*(4), 687–704. https://doi.org/10.4319/lo.1997.42.4.0687

Hartman, S. E., Lampitt, R. S., Larkin, K. E., Pagnani, M., Campbell, J., Gkritzalis, T., et al. (2012). The Porcupine Abyssal Plain fixed-point sustained observatory (PAP-SO): Variations and trends from the northeast Atlantic fixed-point time-series. *ICES Journal of Marine Science*, *69*(5), 776–783. https://doi.org/10.1093/icesjms/fss077

Henson, S. A., Lampitt, R., & Johns, D. (2012). Variability in phytoplankton community structure in response to the North Atlantic Oscillation and implications for organic carbon flux. *Limnology & Oceanography*, *57*(6), 1591–1601. https://doi.org/10.4319/lo.2012.57.6.1591

Henson, S. A., Laufkötter, C., Leung, S., Giering, S. L. C., Palevsky, H. I., & Cavan, E. L. (2022). Uncertain response of ocean biological carbon export in a changing world. *Nature Geoscience*, *15*(4), 248–254. https://doi.org/10.1038/s41561-022-00927-0

Henson, S. A., Le Moigne, F. A. C., & Giering, S. (2019). Drivers of carbon export efficiency in the global ocean. *Global Biogeochemical Cycles*, *33*(7), 891–903. https://doi.org/10.1029/2018GB006158

Henson, S. A., Sanders, R., & Madsen, E. (2012). Global patterns in efficiency of particulate organic carbon export and transfer to the deep ocean. *Global Biogeochemical Cycles*, *26*(1), GB1028. https://doi.org/10.1029/2011GB004099

Henson, S. A., Sanders, R., Madsen, E., Morris, P. J., Le Moigne, F. A. C., & Quartly, G. D. (2011). A reduced estimate of the strength of the ocean's biological carbon pump. *Geophysical Research Letters*, *38*(4), L04606. https://doi.org/10.1029/2011gl046735

Henson, S. A., Yool, A., & Sanders, R. (2015). Variability in efficiency of particulate organic carbon export: A model study. *Global Biogeochemical Cycles*, *29*(1), 33–45. https://doi.org/10.1002/2014GB004965

Herzfeld, M. (2006). An alternative coordinate system for solving finite difference ocean models. *Ocean Modelling*, *14*(3), 174–196. https://doi.org/10.1016/j.ocemod.2006.04.002

Hirst, A. G., Roff, J. C., & Lampitt, R. S. (2003). A synthesis of growth rates in marine epipelagic invertebrate zooplankton. *Advances in Marine Biology*, *44*, 1–142.

Honda, M. C., Kawakami, H., Sasaoka, K., Watanabe, S., & Dickey, T. (2006). Quick transport of primary produced organic carbon to the ocean interior. *Geophysical Research Letters*, *33*(16), L16603. https://doi.org/10.1029/2006GL026466

Irion, S., Christaki, U., Berthelot, H., L'Helguen, S., & Jardillier, L. (2021). Small phytoplankton contribute greatly to CO_2-fixation after the diatom bloom in the Southern Ocean. *The ISME Journal*, *15*(9), 2509–2522. https://doi.org/10.1038/s41396-021-00915-z

Jackson, G. A. (1990). A model of the formation of marine algal flocs by physical coagulation processes. *Deep-Sea Research Part I Oceanographic Research Papers*, *37*(8), 1197–1211. https://doi.org/10.1016/0198-0149(90)90038-W

Jin, D., Hoagland, P., & Buesseler, K. O. (2020). The value of scientific research on the ocean's biological carbon pump. *Science of the Total Environment*, *749*, 141357. https://doi.org/10.1016/j.scitotenv.2020.141357

Johnson, K. S., & Bif, M. B. (2021). Constraint on net primary productivity of the global ocean by Argo oxygen measurements. *Nature Geoscience*, *14*(10), 769–774. https://doi.org/10.1038/s41561-021-00807-z

Joubert, W. R., Thomalla, S. J., Waldron, H. N., Lucas, M. I., Boye, M., Le Moigne, F. A. C., et al. (2011). Nitrogen uptake by phytoplankton in the Atlantic sector of the Southern Ocean during late austral summer. *Biogeosciences*, *8*(10), 2947–2959. https://doi.org/10.5194/bg-8-2947-2011

Karl, D. M., Knauer, G. A., & Martin, J. H. (1988). Downward flux of particulate organic matter in the ocean: A particle decomposition paradox. *Nature*, *332*(6163), 438–441. https://doi.org/10.1038/332438a0

Kawakami, H., & Honda, M. C. (2007). Time-series observation of POC fluxes estimated from ^{234}Th in the northwestern North Pacific. *Deep Sea Research Part I: Oceanographic Research Papers*, *54*(7), 1070–1090. https://doi.org/10.1016/j.dsr.2007.04.005

Kobari, T., Nakamura, R., Unno, K., Kitamura, M., Tanabe, K., Nagafuku, H., et al. (2016). Seasonal variability in carbon demand and flux by mesozooplankton communities at subarctic and subtropical sites in the western North Pacific Ocean. *Journal of Oceanography*, *72*(3), 403–418. https://doi.org/10.1007/s10872-015-0348-7

Lasbleiz, M., Leblanc, K., Armand, L. K., Christaki, U., Georges, C., Obernosterer, I., & Quéguiner, B. (2016). Composition of diatom communities and their contribution to plankton biomass in the naturally iron-fertilized region of Kerguelen in the Southern Ocean. *FEMS Microbiology Ecology*, *92*(11), fiw171. https://doi.org/10.1093/femsec/fiw171

Laurenceau-Cornec, E. C. (2023). Global in situ ocean POC flux compilation dataset [Dataset]. Zenodo. https://doi.org/10.5281/zenodo.8207286

Laurenceau-Cornec, E. C., Trull, T. W., Davies, D. M., Bray, S. G., Doran, J., Planchon, F., et al. (2015a). The relative importance of phytoplankton aggregates and zooplankton fecal pellets to carbon export: Insights from free-drifting sediment trap deployments in naturally iron-fertilised waters near the Kerguelen plateau. *Biogeosciences*, *12*(4), 1007–1027. https://doi.org/10.5194/bg-12-1007-2015

Laurenceau-Cornec, E. C., Trull, T. W., Davies, D. M., De La Rocha, C. L., & Blain, S. (2015b). Phytoplankton morphology controls on marine snow sinking velocity. *Marine Ecology Progress Series*, *520*, 35–56. https://doi.org/10.3354/meps11116

Laws, E. A., & Maiti, K. (2019). The relationship between primary production and export production in the ocean: Effects of time lags and temporal variability. *Deep Sea Research Part I*, *148*, 100–107. https://doi.org/10.1016/j.dsr.2019.05.006

Le Moigne, F. A. C. (2019). Pathways of organic carbon downward transport by the oceanic biological carbon pump. *Frontiers in Marine Science*, *6*, 634. https://doi.org/10.3389/fmars.2019.00634

Le Moigne, F. A. C., Boye, M., Masson, A., Corvaisier, R., Grossteffan, E., Guéneugues, A., & Pondaven, P. (2013). Description of the biogeochemical features of the subtropical southeastern Atlantic and the Southern Ocean south of South Africa during the austral summer of the International Polar Year. *Biogeosciences*, *10*(1), 281–295. https://doi.org/10.5194/bg-10-281-2013

Le Moigne, F. A. C., Henson, S. A., Sanders, R. J., & Madsen, E. (2013). Global database of surface ocean particulate organic carbon export fluxes diagnosed from the ^{234}Th technique. *Earth System Science Data*, *5*(2), 295–304. https://doi.org/10.5194/essd-5-295-2013

Le Moigne, F. A. C., Poulton, A. J., Henson, S. A., Daniels, C. J., Fragoso, G. M., Mitchell, E., et al. (2015). Carbon export efficiency and phytoplankton community composition in the Atlantic sector of the Arctic Ocean. *Journal of Geophysical Research: Oceans*, *120*(6), 3896–3912. https://doi.org/10.1002/2015JC010700

Loeff, M. M. R. V. D., Friedrich, J., & Bathmann, U. V. (1997). Carbon export during the spring bloom at the Antarctic polar front, determined with the natural tracer ^{234}Th. *Deep Sea Research Part II*, *44*(1–2), 457–478. https://doi.org/10.1016/S0967-0645(96)00067-7

Longhurst, A. (2007). *Ecological geography of the sea* (2nd ed.). Academic Press.

Lutz, M. J., Caldeira, K., Dunbar, R. B., & Behrenfeld, M. J. (2007). Seasonal rhythms of net primary production and particulate organic carbon flux to depth describe the efficiency of biological pump in the global ocean. *Journal of Geophysical Research*, *112*(C10), C10011. https://doi.org/10.1029/2006JC003706

Maiti, K., Charette, M. A., Buesseler, K. O., & Kahru, M. (2013). An inverse relationship between production and export efficiency in the Southern Ocean. *Geophysical Research Letters*, *40*(8), 1557–1561. https://doi.org/10.1002/grl.50219

Matsumoto, K., Honda, M. C., Sasaoka, K., Wakita, M., Kawakami, H., & Watanabe, S. (2014). Seasonal variability of primary production and phytoplankton biomass in the western Pacific subarctic gyre: Control by light availability within the mixed layer. *Journal of Geophysical Research: Oceans*, *119*(9), 6523–6534. https://doi.org/10.1002/2014JC009982

Moore, J. K., & Abbott, M. R. (2002). Surface chlorophyll concentrations in relation to the Antarctic polar front: Seasonal and spatial patterns from satellite observations. *Journal of Marine Systems*, *37*(1), 69–86. https://doi.org/10.1016/S0924-7963(02)00196-3

Moore, J. K., Doney, S. C., Glover, D. M., & Fung, I. Y. (2002). Iron cycling and nutrient-limitation patterns in surface waters of the World Ocean. *Deep Sea Research Part II*, *49*(1), 463–507. https://doi.org/10.1016/S0967-0645(01)00109-6

Mouw, C. B., Barnett, A., McKinley, G. A., Gloege, L., & Pilcher, D. (2016). Phytoplankton size impact on export flux in the global ocean. *Global Biogeochemical Cycles*, *30*(10), 1542–1562. https://doi.org/10.1002/2015GB005355

NASA Ocean Biology Processing Group. (2019). Ancillary data sources [Dataset]. NASA. Retrieved from https://oceancolor.gsfc.nasa.gov/

Nowicki, M., DeVries, T., & Siegel, D. A. (2022). Quantifying the carbon export and sequestration pathways of the ocean's biological carbon pump. *Global Biogeochemical Cycles*, *36*(3), e2021GB007083. https://doi.org/10.1029/2021GB007083

Omand, M. M., D'Asaro, E. A., Lee, C. M., Perry, M. J., Briggs, N., Cetinić, I., & Mahadevan, A. (2015). Eddy-driven subduction exports particulate organic carbon from the spring bloom. *Science*, *348*(6231), 222–225. https://doi.org/10.1126/science.1260062

Orsi, A. H., Whitworth, T., III, & Nowlin, W. D., Jr. (1995). On the meridional extent and fronts of the Antarctic Circumpolar Current. *Deep Sea Research Part I*, *42*(5), 641–673. https://doi.org/10.1016/0967-0637(95)00021-W

Ploug, H., Iversen, M. H., Koski, M., & Buitenhuis, E. T. (2008). Production, oxygen respiration rates, and sinking velocity of copepod fecal pellets: Direct measurements of ballasting by opal and calcite. *Limnology & Oceanography*, *53*(2), 469–476. https://doi.org/10.4319/lo.2008.53.2.0469

Prairie, J., Ziervogel, K., Arnosti, C., Camassa, R., Falcon, C., Khatri, S., et al. (2013). Delayed settling of marine snow at sharp density transitions driven by fluid entrainment and diffusion-limited retention. *Marine Ecology Progress Series*, *487*, 185–200. https://doi.org/10.3354/meps10387

Quéguiner, B. (2013). Iron fertilization and the structure of planktonic communities in high nutrient regions of the Southern Ocean. *Southern Ocean Natural Iron Fertilization*, *90*(0), 43–54. https://doi.org/10.1016/j.dsr2.2012.07.024

Rembauville, M., Blain, S., Armand, L., Quéguiner, B., & Salter, I. (2015). Export fluxes in a naturally iron-fertilized area of the Southern Ocean—Part 2: Importance of diatom resting spores and faecal pellets for export. *Biogeosciences*, *12*(11), 3171–3195. https://doi.org/10.5194/bg-12-3171-2015

Reygondeau, G., Longhurst, A., Martinez, E., Beaugrand, G., Antoine, D., & Maury, O. (2013). Dynamic biogeochemical provinces in the global ocean. *Global Biogeochemical Cycles*, *27*(4), 1046–1058. https://doi.org/10.1002/gbc.20089

Richardson, T. L. (2019). Mechanisms and pathways of small-phytoplankton export from the surface ocean. *Annual Review of Marine Science*, *11*(1), 57–74. https://doi.org/10.1146/annurev-marine-121916-063627

Richardson, T. L., & Jackson, G. A. (2007). Small phytoplankton and carbon export from the surface ocean. *Science*, *315*(5813), 838–840. https://doi.org/10.1126/science.1133471

Roca-Martí, M., Puigcorbé, V., Iversen, M. H., Loeff, M. R. V. D., Klaas, C., Cheah, W., et al. (2017). High particulate organic carbon export during the decline of a vast diatom bloom in the Atlantic sector of the Southern Ocean. *Deep Sea Research Part II: Topical Studies in Oceanography*, *138*, 102–115. https://doi.org/10.1016/j.dsr2.2015.12.007

Ross, T., Craig, S. E., Comeau, A., Davis, R., Dever, M., & Beck, M. (2017). Blooms and subsurface phytoplankton layers on the Scotian Shelf: Insights from profiling gliders. *Journal of Marine Systems*, *172*, 118–127. https://doi.org/10.1016/j.jmarsys.2017.03.007

Ruckdeschel, G. S., Davies, K. T. A., & Ross, T. (2020). Biophysical drivers of zooplankton variability on the scotian shelf observed using profiling electric gliders. *Frontiers in Marine Science*, *7*, 627. https://doi.org/10.3389/fmars.2020.00627

Rutgers van der Loeff, M., Cai, P. H., Stimac, I., Bracher, A., Middag, R., Klunder, M. B., & van Heuven, S. M. A. C. (2011). ^{234}Th in surface waters: Distribution of particle export flux across the Antarctic Circumpolar Current and in the Weddell Sea during the GEOTRACES expedition ZERO and DRAKE. *Deep Sea Research Part II: Topical Studies in Oceanography*, *58*(25–26), 2749–2766. https://doi.org/10.1016/j.dsr2.2011.02.004

Schlenger, A. J., Libralato, S., & Ballance, L. T. (2019). Temporal variability of primary production explains marine ecosystem structure and function. *Ecosystems*, *22*(2), 331–345. https://doi.org/10.1007/s10021-018-0272-y

Schmidtko, S., Johnson, G. C., & Lyman, J. M. (2013). MIMOC: A global monthly isopycnal upper-ocean climatology with mixed layers. *Journal of Geophysical Research: Oceans*, *118*(4), 1658–1672. https://doi.org/10.1002/jgrc.20122

Schmoker, C., Hernández-León, S., & Calbet, A. (2013). Microzooplankton grazing in the oceans: Impacts, data variability, knowledge gaps and future directions. *Journal of Plankton Research*, *35*(4), 691–706. https://doi.org/10.1093/plankt/fbt023

Siegel, D. A., Buesseler, K. O., Doney, S. C., Sailley, S. F., Behrenfeld, M. J., & Boyd, P. W. (2014). Global assessment of ocean carbon export by combining satellite observations and food-web models. *Global Biogeochemical Cycles*, *28*(3), GB004743. https://doi.org/10.1002/2013GB004743

Siegel, D. A., Doney, S. C., & Yoder, J. A. (2002). The North Atlantic spring phytoplankton bloom and Sverdrup's critical depth hypothesis. *Science*, *296*(5568), 730–733. https://doi.org/10.1126/science.1069174

Silsbe, G. M., Behrenfeld, M. J., Halsey, K. H., Milligan, A. J., & Westberry, T. K. (2016). The CAFE model: A net production model for global ocean phytoplankton. *Global Biogeochemical Cycles*, *30*(12), 1756–1777. https://doi.org/10.1002/2016GB005521

Smythe-Wright, D., Boswell, S., Kim, Y.-N., & Kemp, A. (2010). Spatio-temporal changes in the distribution of phytopigments and phytoplanktonic groups at the Porcupine Abyssal Plain (PAP) site. *Deep Sea Research Part II: Topical Studies in Oceanography*, *57*(15), 1324–1335. https://doi.org/10.1016/j.dsr2.2010.01.009

Steinberg, D. K., & Landry, M. R. (2017). Zooplankton and the ocean carbon cycle. *Annual Review of Marine Science*, *9*(1), 413–444. https://doi.org/10.1146/annurev-marine-010814-015924

The MathWorks Inc. (2020). Statistics and machine learning toolbox documentation [Software]. Natick, Massachusetts: The MathWorks Inc. Retrieved from https://www.mathworks.com/help/stats/index.html

Thomalla, S. J., Fauchereau, N., Swart, S., & Monteiro, P. M. S. (2011). Regional scale characteristics of the seasonal cycle of chlorophyll in the Southern Ocean. *Biogeosciences*, *8*(10), 2849–2866. https://doi.org/10.5194/bg-8-2849-2011

Torres-Valdés, S., Martin, A. P., Painter, S., & Sanders, R. J. (2013). Compilation of downward flux observations from sediment trap deployments in the Atlantic Ocean—Contribution to EURO-BASIN's Data integration. *PANGAEA*. https://doi.org/10.1594/PANGAEA.807946

Trull, T. W., Bray, S. G., Buesseler, K. O., Lamborg, C. H., Manganini, S., Moy, C., & Valdes, J. (2008). In situ measurement of mesopelagic particle sinking rates and the control of carbon transfer to the ocean interior during the Vertical Flux in the Global Ocean (VERTIGO) voyages in the North Pacific. *Deep-Sea Research Part II Topical Studies in Oceanography*, *55*(14–15), 1684–1695. https://doi.org/10.1016/j.dsr2.2008.04.021

Trull, T. W., Davies, D. M., Dehairs, F., Cavagna, A.-J., Lasbleiz, M., Laurenceau-Cornec, E. C., et al. (2015). Chemometric perspectives on plankton community responses to natural iron fertilisation over and downstream of the Kerguelen Plateau in the Southern Ocean. *Biogeosciences*, *12*(4), 1029–1056. https://doi.org/10.5194/bg-12-1029-2015

Trull, T. W., Jansen, P., Schulz, E., Weeding, B., Davies, D. M., & Bray, S. G. (2019). Autonomous multi-trophic observations of productivity and export at the Australian Southern Ocean time series (SOTS) reveal sequential mechanisms of physical-biological coupling. *Frontiers in Marine Science*, *6*, 525. https://doi.org/10.3389/fmars.2019.00525

Volk, T., & Hoffert, M. I. (1985). Ocean carbon pumps: Analysis of relative strengths and efficiencies in ocean-driven atmospheric CO_2 changes. In *The carbon cycle and atmospheric CO_2: Natural variations Archean to present* (Vol. 32, pp. 99–110). AGU. https://doi.org/10.1029/GM032p0099

Wassmann, P. (1998). Retention versus export food chains: Processes controlling sinking loss from marine pelagic systems. *Hydrobiologia*, *363*(1–3), 29–57. https://doi.org/10.1023/A:1003113403096

Westberry, T., Behrenfeld, M. J., Siegel, D. A., & Boss, E. (2008). Carbon-based primary productivity modeling with vertically resolved photoacclimation. *Global Biogeochemical Cycles*, *22*(2), 1–18. https://doi.org/10.1029/2007GB003078

Wexels Riser, C., Reigstad, M., Wassmann, P., Arashkevich, E., & Falk-Petersen, S. (2007). Export or retention? Copepod abundance, faecal pellet production and vertical flux in the marginal ice zone through snap shots from the northern Barents sea. *Polar Biology*, *30*(6), 719–730. https://doi.org/10.1007/s00300-006-0229-z

Wynn-Edwards, C. A., Shadwick, E. H., Davies, D. M., Bray, S. G., Jansen, P., Trinh, R., & Trull, T. W. (2020). Particle fluxes at the Australian Southern Ocean time series (SOTS) achieve organic carbon sequestration at rates close to the global median, are dominated by biogenic carbonates, and show No temporal trends over 20-years. *Frontiers in Earth Science*, *8*, 329. https://doi.org/10.3389/feart.2020.00329

References From the Supporting Information

Gentleman, W. (2002). A chronology of plankton dynamics in silico: How computer models have been used to study marine ecosystems. *Hydrobiologia*, *480*(1–3), 69–85. https://doi.org/10.1023/A:1021289119442

Straile, D. (1997). Gross growth efficiencies of protozoan and metazoan zooplankton and their dependence on food concentration, predator-prey weight ratio, and taxonomic group. *Limnology & Oceanography*, *42*(6), 1375–1385. https://doi.org/10.4319/lo.1997.42.6.1375